

This is the accepted manuscript made available via CHORUS. The article has been published as:

Supergravity models with 50–100 TeV scalars, supersymmetry discovery at the LHC, and gravitino decay constraints

Amin Aboubrahim and Pran Nath

Phys. Rev. D **96**, 075015 — Published 13 October 2017

DOI: [10.1103/PhysRevD.96.075015](https://doi.org/10.1103/PhysRevD.96.075015)

Supergravity Models with 50-100 TeV Scalars, SUSY Discovery at the LHC and Gravitino Decay Constraints

Amin Aboubrahim* and Pran Nath†

Department of Physics, Northeastern University, Boston, MA 02115-5000, USA

Abstract: We investigate the possibility of testing supergravity unified models with scalar masses in the range 50-100 TeV and much lighter gaugino masses at the Large Hadron Collider. The analysis is carried out under the constraints that models produce the Higgs boson mass consistent with experiment and also produce dark matter consistent with WMAP and PLANCK experiments. A set of benchmarks in the supergravity parameter space are investigated using a combination of signal regions which are optimized for the model set. It is found that some of the models with scalar masses in the 50-100 TeV mass range are discoverable with as little as 100 fb^{-1} of integrated luminosity and should be accessible at the LHC RUN II. The remaining benchmark models are found to be discoverable with less than 1000 fb^{-1} of integrated luminosity and thus testable in the high luminosity era of the LHC, i.e., at HL-LHC. It is shown that scalar masses in the 50-100 TeV range but gaugino masses much lower in mass produce unification of gauge coupling constants, consistent with experimental data at low scale, with as good an accuracy (and sometimes even better) as models with low ($\mathcal{O}(1)$ TeV) weak scale supersymmetry. Decay of the gravitinos for the supergravity model benchmarks are investigated and it is shown that they decay before the Big Bang Nucleosynthesis (BBN). Further, we investigate the non-thermal production of neutralinos from gravitino decay and it is found that the non-thermal contribution to the dark matter relic density is negligible relative to that from the thermal production of neutralinos for reheat temperature after inflation up to 10^9 GeV. An analysis of the direct detection of dark matter for SUGRA models with high scalar masses is also discussed. SUGRA models with scalar masses in the range 50-100 TeV have several other attractive features such as they help alleviate the SUSY CP problem and help suppress proton decay from baryon and lepton number violating dimension five operators.

*Email: a.abouibrahim@northeastern.edu

†Email: p.nath@northeastern.edu

1 Introduction

Supersymmetry (SUSY) has not been observed thus far, which implies that the weak supersymmetry scale is higher than was expected before the Higgs boson [1–3] was discovered at the Large Hadron Collider (LHC) and specifically before the measurement of its mass at ~ 125 GeV [4, 5]. Analyses within high-scale supergravity grand unified models (SUGRA) [6] (for a review see [7]) show that the loop correction to the Higgs boson mass in supersymmetry must be sizable, which in turn implies a value of weak SUSY scale lying in the several TeV region [8–11]. There is another constraint that explains the possible reason for the lack of detection of a supersymmetric signal. In supergravity grand unified models with R-parity conservation, neutralino is the lightest supersymmetric particle (LSP) over most of the parameter space of models [12] and thus a candidate for dark matter. The annihilation of the neutralino in sufficient amounts to have its relic density consistent with the WMAP [13] and the PLANCK [14] experimental results imposes additional constraints. Specifically if the neutralino is bino-like, one needs coannihilation (for early work see [15]) to have consistency with experiment. However, coannihilation implies that the next-to-lightest supersymmetric particle (the NLSP) must be close to the LSP with a small mass gap to ensure efficient annihilation of the LSP. The existence of the small mass gap in turn implies that the final states in the decay of the NLSP will be soft making them difficult to detect.

Coannihilation appears in supergravity models with universal as well as with non-universal boundary conditions at the grand unification scale which lead to a large sparticle landscape [16]. The large landscape includes non-universalities in the gaugino sector [17, 18] and in the matter and Higgs sectors [19]. As mentioned above the measurement of the Higgs boson mass at 125 GeV, implies that the scale of weak scale supersymmetry lies in the several TeV region. Assuming universality of the scalar mass at the GUT scale a high value of the universal scalar mass m_0 is indicated. Quite interestingly it has been previously argued that scalar masses could be large and natural on the hyperbolic branch of radiative breaking of the electroweak symmetry [20–26]. In this analysis we consider much higher values of scalar masses than typically considered in supergravity models, i.e., scalar masses lying in the 50–100 TeV region. This regime of scalar masses help alleviate some of the problems associated with low values of the weak SUSY scale such as the SUSY CP problem (see, e.g., [27]) and fast proton decay from baryon and lepton number violating dimension five operators [28, 29]. Further, in supergravity unified models the gravitino mass $m_{\tilde{G}}$ and the scalar mass m_0 are related and thus a large m_0 in the 50–100 TeV range helps alleviate the problem arising from the late decay of the gravitino which would upset the Big Bang Nucleosynthesis (BBN). In the work of [30, 31] the authors consider a similar model, however, they do not impose the relic density constraint. Also, our work has a more comprehensive study of signatures from LHC and indirect DM search as well as gravitino decay.

The search for supersymmetric signatures in models of the above type with high values of m_0 would necessarily focus on light gauginos and a compressed spectrum. Models with coannihilation and a compressed spectrum have been analyzed over the years in a variety of settings involving chargino, stau, stop and gluino coannihilation (For some recent works on coannihilation related to the analysis here see [32–34]. For other related works see [35–43].

For recent theory papers related to supersymmetry and compressed spectrum see [44–47] and for experimental searches for supersymmetry with a compressed spectrum see [48–50]).

The outline of the rest of the paper is as follows: In section 2 we discuss a set of benchmarks for supergravity models with scalar masses in the 50-100 TeV mass range. The benchmarks are chosen so they satisfy the radiative breaking of electroweak symmetry, give a Higgs boson mass consistent with experiment, and produce a relic density for neutralino cold dark matter consistent with WMAP and PLANCK. In section 3, we compare the gauge coupling unification for supergravity models with low weak scale supersymmetry vs high weak scale supersymmetry consistent with the LEP data. In section 4, we discuss the production of supersymmetric particles and their decays. Here we exhibit the cross sections for the production of the SUSY particle pairs $\tilde{\chi}_2^0\tilde{\chi}_1^\pm$, $\tilde{\chi}_1^+\tilde{\chi}_1^-$, $\tilde{\chi}_1^0\tilde{\chi}_1^\pm$ and $\tilde{g}\tilde{g}$. The sparticles decay with a neutralino and standard model (SM) particles in the final states. The signature analysis of these requires a knowledge of the backgrounds arising from the production and decay of the standard model particles. Here we use the backgrounds published by the SNOWMASS group [51]. Section 5 is devoted to the signature analysis of the benchmarks and an analysis of the minimum integrated luminosity needed at the LHC operating at 14 TeV for the 5σ discovery. Here a comparison of the different signature regions is also made and combined signal region results are exhibited where models are arranged in terms of ascending order in the minimum integrated luminosity needed for a 5σ discovery. In section 6, we discuss the gravitino decay and its possible contribution to the LSP relic density. In section 7, we discuss direct detection of dark matter for SUGRA models with 50-100 TeV scalars. Conclusions are given in section 8.

2 SUGRA models with 50-100 TeV scalar masses

To analyze supergravity models with scalar masses in the range 50-100 TeV, we need to explore the supergravity parameter space consistent with radiative breaking of the electroweak symmetry, the Higgs boson mass and relic density constraints. We are also interested in exploring the parameter space where the gaugino masses are relatively light with masses that would be accessible at the LHC. Further, we limit ourselves to the case that R-parity is conserved so that the LSP is stable. Often in most of the parameter space of supergravity models it is found that under constraints of radiative breaking of the electroweak symmetry the lightest neutralino is the LSP [12], and under the assumption of R-parity conservation, it is a candidate for dark matter. In this case the constraints on dark matter relic density given by WMAP and PLANCK become relevant. It is found that in part of the parameter space, where the Higgs boson mass constraint is satisfied the neutralino turns out to be mostly a bino. The annihilation cross section for the bino-like neutralino is small and thus the neutralinos in the early universe cannot efficiently annihilate themselves to standard model particles to produce the desired relic density. Here one needs coannihilation to reduce the neutralino relic density to be compatible with WMAP and PLANCK data on cold dark matter.

Coannihilation can be easily achieved in supergravity models with non-universal gaugino

masses. One such possibility is non-universality between the $U(1)$ gaugino mass m_1 and the $SU(2)$ gaugino mass m_2 . In this case the light chargino $\tilde{\chi}_1^\pm$ may lie close to the LSP neutralino $\tilde{\chi}_1^0$ which results in coannihilation while the mass of the $SU(3)$ gaugino m_3 is relatively much larger, i.e. $m_3 \gg m_1, m_2$. The parameter space of this model is thus given by $m_0, A_0, m_2 < m_1 \ll m_3$, $\tan\beta, \text{sign}(\mu)$, where A_0 is the universal trilinear scalar coupling at the grand unification scale, $\tan\beta = \langle H_2 \rangle / \langle H_1 \rangle$, where H_2 gives mass to the up quarks and H_1 gives mass to the down quarks and the leptons, and $\text{sign}(\mu)$ is the sign of the Higgs mixing parameter which enters in the superpotential in the term $\mu H_1 H_2$. Using the above input parameters, the sparticle spectrum is generated using **SoftSUSY** 4.0.1 [52, 53] while the analysis of the relic density is done using **micrOMEGAs** 4.3.2 [54]. SUSY Les Houches Accord formatted data files are processed using **PySLHA** [55].

To determine the prospects of SUSY discovery for SUGRA models with high scalar masses, ten benchmark points were generated lying in the mass range 50-100 TeV. The benchmarks selected were those satisfying the radiative electroweak symmetry breaking constraints (for a review see [56]), Higgs boson mass constraint with the Higgs boson mass lying in the range 125 ± 2 GeV. These model points also satisfied the constraint on the relic density of the LSP neutralino so that $\Omega_{\tilde{\chi}_1^0} h^2 < 0.128$. These benchmarks are displayed in Table 1 and the corresponding sparticle masses, the Higgs boson mass and relic density are shown in Table 2. Note that $A_0 \approx 2m_0$ for all the benchmarks consistent with previous works that the large loop correction to the Higgs boson mass requires a substantial A_0 (see, e.g., [8]). Further, on average, $m_2 \approx 0.8m_1$, which is needed to bring the chargino mass close to the LSP mass. The mass gap between the LSP mass and the chargino mass lies in the range ~ 15 to 28 GeV leading to a compressed spectrum for the LSP and the NLSP. The compressed spectrum implies that the decay of the NLSP will lead to soft leptons and jets making the detection of supersymmetry a challenging task for this part of the parameter space.

The benchmarks of Table 1 are used to generate Table 2 which exhibits a set of sparticle masses including the light spectrum as well as the heaviest squark and the average sfermion mass. The heaviest squark has a mass roughly m_0 , whereas the average sfermion mass appears to be lower than m_0 . The reason for the average sfermion mass being lower than m_0 is due to the presence of lighter third generation squarks (see Fig. 4) where the analysis is done using **softSUSY**. In the regime of m_0 in the range 50-100 TeV, spectrum generators tend to be less stable. This arises from convergence problems mainly due to μ becoming highly dependent on the top Yukawa coupling [57]. Using **softSUSY**, we have made sure that none of the points considered in this analysis suffer from such a convergence problem. Further, model points have been cross tested using **ISAJET** [58] which gives a spectrum within the same mass range as **softSUSY**. We note in passing that the parameter set of Table 1 has not been ruled out by experiment, as can be seen by comparing the spectrum of Table 2 with the $\tilde{\chi}_1^\pm - \tilde{\chi}_1^0$ or the $\tilde{\chi}_1^\pm - \tilde{g}$ exclusion plots from experiment [59–61].

3 Gauge coupling unification with high mass scalars

One of the well known successes of SUSY is that it gives a unification of gauge couplings consistent with LEP data [62]. In such analyses the typical assumption made is of sparticle masses in the sub-TeV-TeV range. In the analysis of Table 2 we find a split sparticle spectrum where the gauginos, $\tilde{\chi}_1^0, \tilde{\chi}_2^0, \tilde{\chi}_1^\pm, \tilde{g}$ have low masses while the scalars are 50-100 times larger in mass. It is then of interest to ask if the unification of gauge couplings holds to the same degree of accuracy for the models of Table 2 as compared to models with all sparticle masses low lying in the sub-TeV-TeV range. To check this, we plot the running of $\alpha_i^{-1} (i = 1, 2, 3)$ ($\alpha_i = g_i^2/4\pi$, where g_i are the gauge couplings for the gauge groups $U(1)_Y, SU(2)_L, SU(3)_C$ and $g_1 = \sqrt{\frac{5}{3}}g_Y$) for model point (j) using **softSUSY**. Fig. 1 shows two plots: The plot on the left exhibits the running of α_i^{-1} for a small universal scalar mass $m_0 = 740$ GeV with all other parameters the same as in Table 1 for point (j). Defining the GUT scale as the bi-junction where α_1 and α_2 meet, one finds that α_3 misses the bi-junction by 3.6 %. The plot on the right exhibits the running of α_i^{-1} with all parameters the same as in Table 1 for point (j). Here one finds that α_s misses the bi-junction by 1.7 %. Thus one finds that unification of gauge couplings occurs to a good accuracy in each case with the larger m_0 case showing a small improvement in this case. A similar result is observed for other model points of Table 1. Thus we conclude that models with scalar masses in the 50-100 TeV range and gaugino masses much lower produce unification of gauge couplings with about the same degree of accuracy as sub-TeV-TeV scale SUSY models and in some cases with a slight improvement.

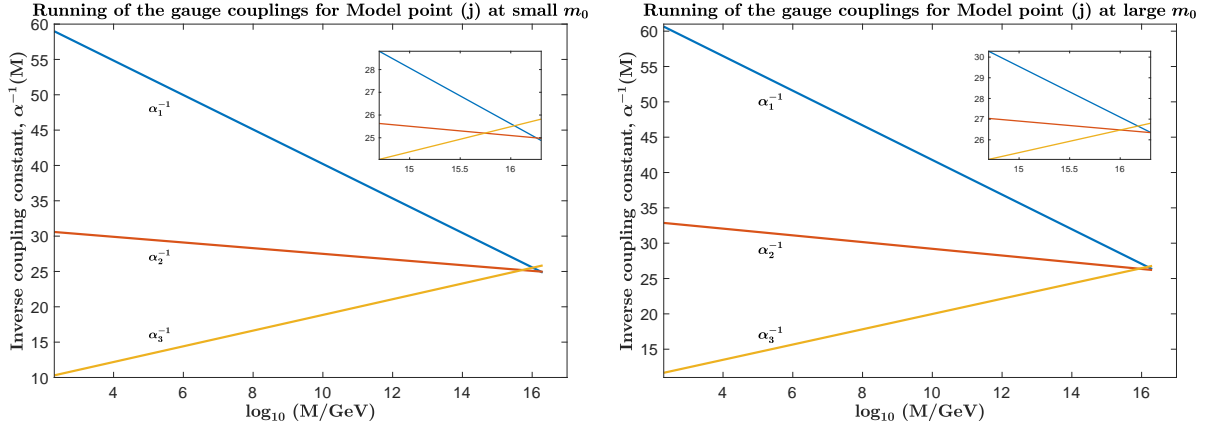


Figure 1: A comparison of the unification of gauge couplings for low scale and high scale SUSY models for the benchmark (j) of Table 1. Left panel: the plot shows the running of $\alpha_i^{-1} (i = 1, 2, 3)$ for $U(1)_Y, SU(2)_L, SU(3)_C$ for low scale SUSY with universal scalar mass $m_0 = 740$ GeV and all other parameters the same as for benchmark (j) in Table 1, where α_s misses the bi-junction where α_1 and α_2 meet by ~ 3.6 %. Right panel: the plot shows the running of α_i^{-1} for the high scale SUSY with universal scalar mass $m_0 = 74$ TeV and all other parameters the same as in the left panel. Here α_s misses the bi-junction by ~ 1.7 %. Thus in this case the high scale SUSY shows a small improvement in the unification fit relative to low scale SUSY.

4 LHC sparticle production and decay at 14 TeV

The benchmarks listed in Table 1 are used in further Monte Carlo analysis in the signal regions appropriate for the detection of a supersymmetric signal at the LHC. This analysis was performed with **MADGRAPH 2.5.5** [63]. First, the Feynman diagrams were calculated for all possible decays of the form $pp \rightarrow \text{SUSY SUSY}$, where “SUSY” can be any R parity odd minimal supersymmetric standard model (MSSM) particle. With the sparticle spectra of the benchmarks calculated by **SoftSUSY 4.0.1**, as well as the decay widths and branching ratios computed by **SDECAY** and **HDECAY** operating within **SUSY-HIT** [64], **MADEVENT** was used to simulate 50,000 MSSM decay events for each benchmark point. Hadronization of resultant particles is handled by **PYTHIA8** [65] where ISR and FSR jets are switched on, and ATLAS detector simulation and event reconstruction is performed by **DELPHES 3.4.1** [66]. A large set of search analyses were performed on the generated events for each benchmark point. The analyses used **ROOT 6.08.06** [67] to implement the constraints of the search region for the signal regions involving leptons, jets and missing transverse energy in the final state.

To allow comparison to the background, all of the signal region analyses were applied to pre generated backgrounds published by the SNOWMASS group [51]. For each benchmark, a calculated implied integrated luminosity allowed direct comparison to the backgrounds. Each individual background process from the SNOWMASS set was scaled by its own implied integrated luminosity and combined to determine a total background count for each signal region. The various background samples are grouped according to the generated final state, with a collective notation given by

$$\begin{aligned} J &= \{u, \bar{u}, d, \bar{d}, s, \bar{s}, c, \bar{c}, b, \bar{b}\}, \quad L = \{e^+, e^-, \mu^+, \mu^-, \tau^+, \tau^-, \nu_e, \nu_\mu, \nu_\tau\}, \\ B &= \{W^+, W^-, Z, \gamma, h^0\}, \quad T = \{t, \bar{t}\}, \quad H = \{h^0\}. \end{aligned} \quad (1)$$

In general, events with gauge bosons and the SM Higgs boson in the final state are grouped into a single “boson” (B) category. Thus, for example, the data set “Bjj-vbf” represents production via vector boson fusion of a gauge boson or a Higgs boson with at least two additional light-quark jets. The standard model background is displayed for two kinematic variables $M_{\text{eff}}(\text{incl.})$ and E_T^{miss} in Fig. 3.

In the analysis, production of all allowed particles in the final state for a given model point is carried out using **MADGRAPH** at a center-of-mass energy of 14 TeV. The choice of 14 TeV rather than the current LHC 13 TeV-run energy is dictated by the SNOWMASS backgrounds used in this analysis which have been generated at 14 TeV. The cross-sections for all the model points of Table 1 are dominated by the production of $\tilde{\chi}_2^0 \tilde{\chi}_1^\pm$ and $\tilde{\chi}_1^+ \tilde{\chi}_1^-$ pairs. A non-negligible production of $\tilde{\chi}_1^0 \tilde{\chi}_1^\pm$ pair is seen in most of the model points, while gluino production is greatly suppressed. A list of the different production cross-sections is shown in Table 3. The myriad of the subsequent decay topologies following the production of the SUSY particles are the target of the signal region definitions and event selection chosen to enhance the signal-to-background ratio. The first signal region is based on jets and missing transverse energy with zero leptons in the final state. As Tables 4 and 5 indicate, the decays of the heavy neutralino and the chargino into jets and missing energy have the largest branching ratios among the other decays. The second set of signal regions is designed

to search for leptons, jets and missing transverse energy in the final state. One of the signal regions in this set looks for a single lepton and the other for two leptons. The latter comes in two categories based on the flavor and charge of the leptons, namely, a pair of leptons having same flavor and opposite sign for the first category while the second looks for a pair with different flavor and opposite sign.

Even though the signal regions used here are inspired by those from ATLAS and CMS analyses, the cuts and event selection for our analysis are fully optimized to capture final states for the chargino coannihilation scenario whereby the mass gap between the chargino (and second neutralino) and the LSP is small and thus results in soft final states.

5 Event selection and results

Based on the character of the final states, event selection proceeds by employing a set of discriminating variables on the signal and SM background. Those variables have been optimized to give the best signal-to-background ratio by imposing tighter requirements on those variables so they are more sensitive to smaller mass gaps between the chargino and the LSP. The signal regions (SR) used in this analysis belong to three main categories: the zero lepton channel, the single lepton and the two lepton channels along with jets, namely, $0\ell nj$, $1\ell nj$ and $2\ell nj$, where n represents the minimum number of jets in the final state. The variety of SRs used have been inspired by analyses done by ATLAS and CMS [61, 68–70] and have been improved for the parameter sets of this work.

5.1 Zero lepton channel

The first signal region we investigate is the one that targets jets and missing transverse energy in the final state with a veto on all leptons (electrons and muons). This signal region, SR- $0\ell nj$, comprises of two signal regions based on the minimum number of jets in the final state, namely $0\ell 2j$ and $0\ell 4j$, with a minimum of 2 and 4 jets, respectively. The leading jets are required to have $p_T > 40$ GeV and all sub-leading jets have $p_T > 20$ GeV. A pre-cut of 100 GeV on the missing transverse energy, E_T^{miss} , is applied to the backgrounds and the signal. Table 6 shows the set of kinematic variables used in this signal region. Cuts are applied on the transverse momenta of jets j_1 , j_2 and j_4 with an upper bound as high as 100 GeV for the leading jet. Jets are produced following the decay of a chargino or second neutralino to the LSP and with the available mass gap between the parent and daughter particles of up to 28 GeV, the extra kick in energy is evidently coming from ISR and FSR. We have two requirements on the azimuthal angle between any jet and the missing transverse energy, one is between the leading jet and the missing transverse energy, $\Delta\phi(\text{jet}_1, E_T^{\text{miss}})$, and the other is the smallest azimuthal separation between the same two objects, $\min[\Delta\phi(\text{jet}_{1-2}, E_T^{\text{miss}})]$. The latter is a good discriminator since background events from multi-jet processes tend to have a small value for this variable. The kinematic variable m_{T2} [71–73] is used on the $0\ell 2j$

signal region, which is defined as

$$m_{T2} = \min \left[\max \left(m_T(\mathbf{p}_T(j_1), \mathbf{q}_T), m_T(\mathbf{p}_T(j_2), \mathbf{p}_T^{\text{miss}} - \mathbf{q}_T) \right) \right], \quad (2)$$

where \mathbf{q}_T is an arbitrary vector chosen to find the appropriate minimum and m_T is the transverse mass given by

$$m_T(\mathbf{p}_{T1}, \mathbf{p}_{T2}) = \sqrt{2(p_{T1} p_{T2} - \mathbf{p}_{T1} \cdot \mathbf{p}_{T2})}. \quad (3)$$

The minimum of the transverse masses of the jets and missing transverse energy, $m_T^{\min}(\text{jet}_{1-2}, E_T^{\text{miss}})$, proves to be a good discriminator for the $0\ell 4j$ SR which reduces W +jets and $t\bar{t}$ background events, along with the effective mass, m_{eff} defined as

$$m_{\text{eff}} = \sum_{i \leq 4} (p_T^{\text{jets}})_i + E_T^{\text{miss}}. \quad (4)$$

The kinematic variable m_{jj} is the invariant mass of the two leading jets and is used in the $0\ell 2j$ SR. Finally the variable $E_T^{\text{miss}}/\sqrt{H_T}$ uses H_T defined as the scalar sum of the transverse momenta of all jets with a lower bound of 100 GeV being set on this variable for the SR $0\ell 2j$ and 110 GeV for SR $0\ell 4j$. All the selection criteria appearing in table 6 have been optimized to give the best minimum integrated luminosity for a 5σ discovery. The different SRs labelled A, B and C correspond to a variation of the kinematic variables $E_T^{\text{miss}}/\sqrt{H_T}$ and H_T for $0\ell 2j$ and H_T for $0\ell 4j$.

The results obtained for the zero lepton channel with a minimum of 2 and 4 jets are shown in Table 7, where entries with three dots indicate that the required integrated luminosity exceeds 3000 fb^{-1} which is the maximum value expected to be reached by the high luminosity LHC (HL-LHC). The distribution of integrated luminosities for the SR $0\ell 2j$ ranges from 83 fb^{-1} for point (e) in $0\ell 2j$ -A to 3000 fb^{-1} for point (h) in $0\ell 2j$ -C, while for $0\ell 4j$ we have a low of 63 fb^{-1} for point (g) in $0\ell 4j$ -A and a high of 2960 fb^{-1} for point (j) also in $0\ell 4j$ -A. Out of the ten points, six of them are visible in all variations of both signal regions.

Figs. 5-7 show some distributions in select kinematic variables used in SRs $0\ell 2j$ and $0\ell 4j$. In Fig. 5 distribution in the azimuthal separation between the leading jet and the missing energy, $\Delta\phi(\text{jet}_1, E_T^{\text{miss}})$, and distribution in the dijet invariant mass, m_{jj} , are plotted for point (a) in the SR $0\ell 2j$ -A at 86 fb^{-1} . In $\Delta\phi(\text{jet}_1, E_T^{\text{miss}})$ the signal is above the background for larger values of this variable. Applying cuts at higher values of $\Delta\phi(\text{jet}_1, E_T^{\text{miss}})$ minimizes any misidentification of missing transverse momentum with jets. The distribution in m_{jj} shows an excess of the signal above background for smaller values of this variable which is an indication of soft final states. This can also be seen in the distribution of the transverse momentum of the leading jet, $p_T(j_1)$, depicted in the left panel of Fig. 6. As noted before, the extra kick is due to contributions from ISR and FSR jets. The right panel shows the distribution of the variable $E_T^{\text{miss}}/\sqrt{H_T}$ for point (e) at 83 fb^{-1} in the same SR. In Fig. 7 we exhibit three distributions in the variables E_T^{miss} , m_T^{\min} and H_T for model point (b) at 1290 fb^{-1} in $0\ell 4j$ -C. The excess of the signal over the background is not as pronounced as in the examples before which is why this point requires a higher integrated luminosity for discovery in this particular SR.

5.2 Single lepton channel

Another SUSY signature to be discussed is the presence of a single isolated lepton in the final state coming from the decay of a chargino, along with jets and missing transverse energy. The signal region used here is labeled $1\ell 2j$, where $2j$ indicates a minimum of two jets in the final state. Events are selected based on one tight electron or muon with $|\eta| < 1.4$ for electrons and $|\eta| < 1.2$ for muons. The azimuthal angle between the emitted lepton momentum and the missing energy is taken as $\Delta\phi(\vec{\ell}, \vec{p}_T^{\text{miss}}) > 1.5$ radians for the electrons and $\Delta\phi(\vec{\ell}, \vec{p}_T^{\text{miss}}) < 1.0$ radians for the muons. As for jets, it is required that the leading and the sub-leading jets both have $p_T > 20$ GeV. The other selection criteria for this SR are listed in Table 8, where a 100 GeV pre-cut is also applied on E_T^{miss} . Here m_T^ℓ is the transverse mass of the lepton and \vec{p}_T^{miss} and m_{eff} is given by

$$m_{\text{eff}} = p_T^\ell + \sum_{i \leq 2} (p_T^{\text{jets}})_i + E_T^{\text{miss}}. \quad (5)$$

The SRs A, B and C correspond to a variation of the transverse momentum of the leading jet. The minimum integrated luminosity for discovery is shown in Table 9. It is clear that this SR is less successful than the previous one, with only 6 points being visible. The integrated luminosity ranges from 80 fb^{-1} for point (a) in $1\ell 2j$ -C to 2780 fb^{-1} for point (g) in $1\ell 2j$ -B and C. In Fig. 8 we exhibit the distributions in the leptonic transverse mass, m_T^ℓ and the leading lepton transverse momentum, p_T^ℓ for model point (c) in SR $1\ell 2j$ -A at 2230 fb^{-1} . Also here, the excess is over small values of those variables which explains the tight cuts applied in this SR.

5.3 Two lepton channel

The last signal region we investigate is the presence of two leptons in the final state coming from the decay of the electroweakinos along with at least one jet. Events containing two leptons are selected such that the leading and the sub-leading lepton transverse momenta must be $p_T^\ell > 15$ GeV and 10 GeV, respectively. A veto on b-tagged jets is applied to reduce $t\bar{t}$ background events. This signal region, $2\ell 1j$, contains two categories of SRs, one which looks for two leptons with same flavor and opposite sign (SFOS) and the other targets two leptons with different flavor and opposite sign (DFOS). For short, we label them as SF and DF. The kinematic variables used and the corresponding cuts are shown in Table 10, where $\Delta R_{\ell\ell}$ and $m_{\ell\ell}$ represent, respectively, the separation between two SF or DF leptons and the invariant mass of those leptons. The cut on $m_{\ell\ell}$ ensures that background events corresponding to leptons coming from the decay of a Z boson are reduced. The three signal regions A, B and C for each category correspond to the variation of the transverse mass m_{eff} defined by

$$m_{\text{eff}} = \sum_{i \leq 2} (p_T^\ell)_i + p_T(j_1) + E_T^{\text{miss}}. \quad (6)$$

In order to reduce possible multi-jet backgrounds we use the variable E_T^{miss}/H_T which is crucial in this SR. A series of optimizations have been carried out on this variable in order

to reduce as much of the background as possible and retain as much of the signal as possible. Such optimization procedures are found useful in exploring atypical regions of the parameter space which could otherwise be missed (see, e.g., [32–34, 74]). The resulting integrated luminosities for a 5σ discovery are listed in Table 11 for the 10 benchmark points. The signal region $2\ell 1j$ -DF has a poor performance compared to $2\ell 1j$ -SF and thus has been eliminated. An integrated luminosity as low as 93 fb^{-1} is obtained for point (b) in $2\ell 1j$ -SF-C and a high of 2800 fb^{-1} for point (j) also in $2\ell 1j$ -SF-C. We exhibit in Fig. 9 the distributions in the dilepton invariant mass, $m_{\ell\ell}$, and the effective mass m_{eff} . In the left panel, $m_{\ell\ell}$ is shown for model point (c) in $2\ell 1j$ -SF-C at 1590 fb^{-1} . One can notice a major dip in the background events for $m_{\ell\ell} < 10 \text{ GeV}$ and so cutting on this variable greatly improves the signal-to-background ratio. Another tight cut is applied on m_{eff} whose distribution is shown on the right panel for model point (d) at 334 fb^{-1} . The signal is above background over a very narrow region which is again indicative of soft final states.

5.4 Combined signal region results

We combine now the results obtained thus far from the different signal regions used for analyzing the discovery potential of the supersymmetric models at the LHC. Table 12 shows the combined results with the leading and the sub-leading SRs and the corresponding integrated luminosities for a 5σ discovery along with their uncertainties. A discussion of the those uncertainties is given in section 5.5. By the end of the LHC run II, ATLAS and CMS are expected to collect around 100 fb^{-1} of data each. From Table 12 we find that the parameter points, (a), (b), (e) and (g), would be within reach by the end of run II. Further, all of the remaining parameter points of Table 12 will be discoverable in the high luminosity era of the LHC (HL-LHC) which is expected to reach its optimal integrated luminosity of 3000 fb^{-1} at $\sqrt{s} = 14 \text{ TeV}$.

5.5 Estimate of uncertainties

Here we discuss the sources of systematic uncertainties that affect the signal and the standard model background and give a rough estimate of them on the predicted integrated luminosities for discovery in Table 12. Theoretical systematic uncertainties for the signal and background arise from scale variation (renormalization and factorization scales), central scheme variation and Parton Distribution Function (PDF) variation. Using **Madgraph** we estimate the theoretical systematic uncertainty to be ~ 6 to $\sim 8\%$. Further, Monte-Carlo statistics adds an uncertainty of $\sim 5\%$ to the signal and $\sim 10\%$ to the background. Common experimental uncertainties are due to Drell-Yan processes ($\sim 5\%$) and diboson production ($\sim 10\%$). The largest contributions to experimental uncertainties are from jet energy scale (JES) and resolution (JER). Based on [60, 61, 68, 69], we estimate the uncertainty from JES (JER) to be $\sim 3\%$ ($\sim 8\%$) for SR- $0\ell 2j$, $\sim 10\%$ ($\sim 12\%$) for SR- $0\ell 4j$, $\sim 2\%$ ($\sim 9\%$) for SR- $1\ell 2j$ and $\sim 13\%$ ($\sim 23\%$) for SR- $2\ell 1j$ -SF. The statistical uncertainty in the cross-sections calculated at LO for the signal and NLO for the background is $\sim 1\%$. Combining all sources of systematic uncertainties on signal and background, we tabulate the results for each signal

region in Table 13. Using the systematics in Table 13, we determine the uncertainty in the predicted integrated luminosities for discovery for the leading and sub-leading SRs. The results are shown in Table 12. The analysis of Table 12 shows that we have $\sim 11\%$ systematic uncertainty in integrated luminosity in the signal regions $0\ell 2j$ and $1\ell 2j$, $\sim 13\%$ for $0\ell 4j$ and $\sim 17\%$ for $2\ell 1j$ -SF. It can be seen that despite the uncertainties our conclusion regarding the possible discovery of some of the points with integrated luminosity as low as 100 fb^{-1} still holds. Table 12 shows that points (a), (b), (e) and (g) could be discovered with an integrated luminosity of 100 fb^{-1} .

5.6 Importance of optimized cuts

Here we try to explain further the importance of implementing optimized cuts in the analysis of supersymmetric signals for a compressed spectrum. The current cumulative luminosity achieved by ATLAS and CMS is $\sim 35 \text{ fb}^{-1}$ and using our choice of cuts gives an estimate of an excess of size $\sim (2 - 3)\sigma$ for the points (a), (b), (e) and (g) which means that some corresponding excess should have been seen for these cases but no such excess is reported in any of the LHC analyses. The question then is if the points (a), (b), (e) and (g) are already excluded by LHC data to date. To investigate this, we utilize the exact signal regions used by ATLAS on our benchmark points and check whether an excess in signals could be seen. We emphasize again that our signal regions have been optimized to target our final states in a compressed spectrum scenario while the LHC analyses are often done in simplified models. We start with the signal region $0\ell 4j$ which is the leading SR for point (g). We implement the ATLAS SR in [68] labelled [Meff] 4j-1000 which also looks for at least four jets in the final state and a veto on the leptons. We run this SR on all our benchmark points which results in zero events passing the cuts. The reason is the hard cuts which are not compatible with our soft final states. The second SR is $1\ell 2j$ where we implement the ATLAS SR in [69] labelled b1L-SRax which looks for one lepton and jets in the final state. Also here we notice that no events pass those cuts for the same reason mentioned for $0\ell 4j$. Next, we examine the SR $0\ell 2j$ and implement the ATLAS SR in [68] labelled [Meff] 2j-1200. This SR looks for at least 2 jets in the final state and a veto on leptons with a hard cut on $m_{\text{eff}}(\text{incl.})$. This SR does produce a 5σ discovery potential for the benchmark points but with integrated luminosities far beyond those attainable by LHC run II. Thus for point (a) which has $0\ell 2j$ as its sub-leading SR, we get an integrated luminosity of 1660 fb^{-1} and for point (e) 6680 fb^{-1} . The value obtained for point (e) is far beyond the HL-LHC. The rest of the points have an integrated luminosity range from 2020 fb^{-1} for point (g) to 16900 fb^{-1} for point (c) for 5σ discovery. The estimated excess will be smaller than 1σ and hence cannot be extracted with the current integrated luminosity. Finally, for SR $2\ell 1j$ -SF we implement the ATLAS SR in [60] labelled SR2 ℓ . The only points that have events passing the cuts are points (g), (i) and (j) with integrated luminosities $\sim 10^4 \text{ fb}^{-1}$. The analysis above shows that applying the signal regions used by ATLAS on our benchmark points require integrated luminosities for 5σ discovery that are in the HL-LHC range and even beyond, which points to the need for optimizing the relevant SRs as we have done in this analysis. The above underlines the importance of using optimized cuts in the analysis of the set of Table 1.

6 The gravitino decay constraints

It is known that stable gravitinos produced in the early universe could overclose the universe if the gravitino mass exceeds 1 keV [75]. Unstable gravitinos also produce cosmological constraints. Since the gravitinos couple with the standard model fields gravitationally, they are long-lived and their decays could upset the BBN if they occur during or after the BBN time, i.e., $(1-10^2)$ s. Of course the primordial gravitinos are all inflated away during inflation but they can be regenerated in the reheating period after inflation. So we need to check the lifetime of the gravitinos for the benchmarks of Table 1. A gravitino has many decay final states to the MSSM states which include the dominant two body decays

$$\tilde{G} \rightarrow \tilde{g}g, \tilde{\chi}_1^\pm W^\mp, \tilde{\chi}_1^0 \gamma, \tilde{\chi}_1^0 Z. \quad (7)$$

In a general set up of supergravity models, there is no direct equality of the gravitino mass and the scalar masses since the scalar masses could in general be nonuniversal depending on the form of the Kahler potential. However, here we make the simple assumption of the universality of the scalar masses at the GUT scale and the equality of the gravitino and the scalar mass, i.e., $m_{\tilde{G}} = m_0$. We point out, however, that scalar masses at the electroweak scale can differ significantly from their values at the GUT scale as a result of renormalization group evolution. Thus from Table 2 we see that the masses of the scalars below the GUT scale are typically smaller than m_0 in the mass range investigated in Table 1. In Table 14 we exhibit the branching ratios of the leading gravitino decay channels of Eq. (7) along with the total decay width and the lifetime of the gravitino for the benchmarks of Table 1, where we have used the code **GravitinoPack** [76, 77]. Table 14 shows that for the benchmark of Table 1 the gravitino decays before the BBN time and thus BBN is not disturbed.

However, there is still one further constraint from an unstable gravitino. Thus, although the gravitinos decay before BBN, their decays produce neutralinos and if there is an overproduction of the gravitinos in the post inflationary period, their decay could generate a neutralino relic density in excess of what is observed. Thus the relic density of neutralinos produced in the decay of the gravitinos acts as a constraint on the model. So now we have the result that the total relic density of neutralinos is

$$\Omega_{\tilde{\chi}_1^0} = \Omega_{\tilde{\chi}_1^0}^{\text{th}} + \Omega_{\tilde{\chi}_1^0}^{\tilde{G}}, \quad (8)$$

where the first term on the right hand side is from the conventional thermal production of neutralinos after freeze out and the second term is from the non-thermal contribution arising from the decay of the gravitino. Under the assumption that each gravitino decay results in just one neutralino we have

$$\Omega_{\tilde{\chi}_1^0}^{\tilde{G}} = \frac{m_{\tilde{\chi}_1^0}}{m_{\tilde{G}}} \Omega_{\tilde{G}}. \quad (9)$$

Thus a computation of $\Omega_{\tilde{\chi}_1^0}^{\tilde{G}}$ requires a computation of $\Omega_{\tilde{G}}$ which depends on particulars of inflation and specifically on the reheat temperature. Thus after the end of inflation, the inflaton field ϕ begins to execute oscillations around the potential minimum. In a simplified

treatment one makes the approximation that the coherent energy of the inflaton is converted instantaneously into radiation energy at a time when the Hubble parameter $H \sim \Gamma_\phi$, where Γ_ϕ is the decay width of the inflaton field ϕ [78]. Thus one has the relation

$$\rho_R = \rho_\phi|_{H=\Gamma_\phi}, \quad (10)$$

where ρ_ϕ is the energy density which on using the Friedmann equations in an FRW universe with zero curvature is given by

$$\rho_\phi = \frac{3}{8\pi G_N} H^2, \quad (11)$$

where G_N is Newton's constant. Further, in Eq. (10) ρ_R is the radiation density which at the reheat temperature $T = T_R$ is given by

$$\rho_R = \frac{\pi^2}{30} g_* T_R^4, \quad (12)$$

where g_* is the number of degrees of freedom at the reheat temperature T_R which for MSSM is $g_* = 228.75$. Defining $M_{\text{Pl}} = (\sqrt{8\pi G_N})^{-1/2}$ where M_{Pl} is the reduced Planck constant $M_{\text{Pl}} \simeq 2.4 \times 10^{18}$ GeV in Eq. 11 and using Eq. 10 one gets an expression for the reheat temperature

$$T_R = \left(\frac{90}{\pi^2 g_*} \right)^{1/4} \sqrt{\Gamma_\phi M_{\text{Pl}}}. \quad (13)$$

The above equation shows that the reheating depends on the details of the inflation model and specifically through the decay width of the inflaton. However, here we will not go into the specifics of inflation models, of which there are many, but rather use the reheat temperature as our starting point which controls the thermal production of the gravitinos. Of course the gravitinos can also be produced by the decays of the inflaton, but again the branching ratio of the inflaton into the gravitino is model dependent. For that reason we will focus on the thermal production of the gravitinos.

The thermal production of gravitinos has been discussed in a variety of papers. A brief list of these include [79–87]. Other work regarding the gravitino decay problem and production which are model-dependent include [88–90]. In supersymmetric QCD the processes that produce the gravitino include

$$g\tilde{g} \rightarrow g\tilde{G}, \quad g\tilde{q} \rightarrow q\tilde{G}, \quad q\bar{q} \rightarrow \tilde{g}\tilde{G}, \dots \quad (14)$$

In addition there are annihilation processes such as $\tilde{G}\tilde{G} \rightarrow f\bar{f}, \tilde{g}\tilde{g}$. However, we will ignore these back reactions since the gravitinos decouple at a temperature $\sim 10^{14}$ GeV, and thus they are decoupled from the thermal bath at the reheat temperatures we consider below which are significantly lower than the gravitino decoupling temperature. It is found that the gravitino production cross section is proportional to the sum of two terms, one from the production of $\pm 3/2$ helicity states and the other from the production of $\pm 1/2$ helicity

states. Thus the Boltzmann equation governing the thermal production of gravitinos after reheating is given by

$$\frac{dn_{\tilde{G}}}{dt} + 3Hn_{\tilde{G}} = a_{\tilde{G}}, \quad (15)$$

where [85]

$$a_{\tilde{G}} = \frac{3\zeta(3)T^6}{16\pi^3 M_{\text{Pl}}^2} \sum_{i=1}^3 c_i g_i^2 \left(1 + \frac{m_i^2}{3m_{\tilde{G}}^2} \right) \ln \left(\frac{k_i}{g_i} \right). \quad (16)$$

Here m_i ($i = 1, 2, 3$) are the gaugino masses for the gauge groups $U(1)_Y$, $SU(2)_L$ and $SU(3)_C$ and g_i are the corresponding gauge coupling constants where m_i and g_i are evaluated at temperature T . Further, $c_i = (11, 27, 72)$ and $k_i = (1.266, 1.312, 1.271)$. We note that Eq. (16) contains the factor

$$\frac{1}{M_{\text{Pl}}^2} \left(1 + \frac{m_i^2}{3m_{\tilde{G}}^2} \right). \quad (17)$$

The significance of this factor is the following: the first term in the brace arises from the production of the $\pm 3/2$ helicity states of the gravitino while the second term in the brace arises from the production of $\pm 1/2$ helicity components. Note that the term that arises from $\pm 3/2$ helicities is independent of m_i and $m_{\tilde{G}}$ while the term that arises from $\pm 1/2$ helicities is dependent on both m_i and $m_{\tilde{G}}$.

Eq. 15 can be solved analytically under the assumption of conservation of entropy per co-moving volume [81]. Here we use Eq.(3) of [85] in Eq. 9 to obtain the neutralino relic density arising from the decay of the gravitino so that

$$\Omega_{\tilde{\chi}_1^0} h^2 = \sum_{i=1}^3 \omega_i g_i^2 \left(1 + \frac{m_i^2}{3m_{\tilde{G}}^2} \right) \ln \left(\frac{k_i}{g_i} \right) \left(\frac{m_{\tilde{\chi}_1^0}}{100 \text{ GeV}} \right) \left(\frac{T_R}{10^{10} \text{ GeV}} \right). \quad (18)$$

Here $\omega_i (i = 1, 2, 3) = (0.018, 0.044, 0.177)$ [85] and m_i and g_i are evaluated at temperature T_R . They can be obtained from their GUT values by using the relations

$$\begin{aligned} \frac{m_i(T_R)}{m_i(M_G)} &= \frac{g_i^2(T_R)}{g_i^2(M_G)}, \\ \frac{1}{g_i^2(T_R)} &= \frac{1}{g_i^2(M_G)} + \frac{\beta_i^{(i)}}{8\pi^2} \ln \left(\frac{M_G}{T_R} \right). \end{aligned} \quad (19)$$

Here M_G is the GUT scale, $g_i(T_R), m_i(T_R)$ are the gauge couplings and the gaugino masses at T_R , and $g_i(M_G), m_i(M_G)$ are their GUT values, $\beta_i^{(1)}$ are the one loop evolution coefficients given by $\beta_i^{(1)} (i = 1, 2, 3) = (11, 1, -3)$. Numerical result of the relic density of neutralinos produced via decay of the gravitino vs the reheat temperature T_R is exhibited in Fig 2. All the model points given in Table 1 lie on the thin blue line. The insensitivity of the neutralino relic density to the gravitino mass is easily understood from Eq. 18 since the relic density

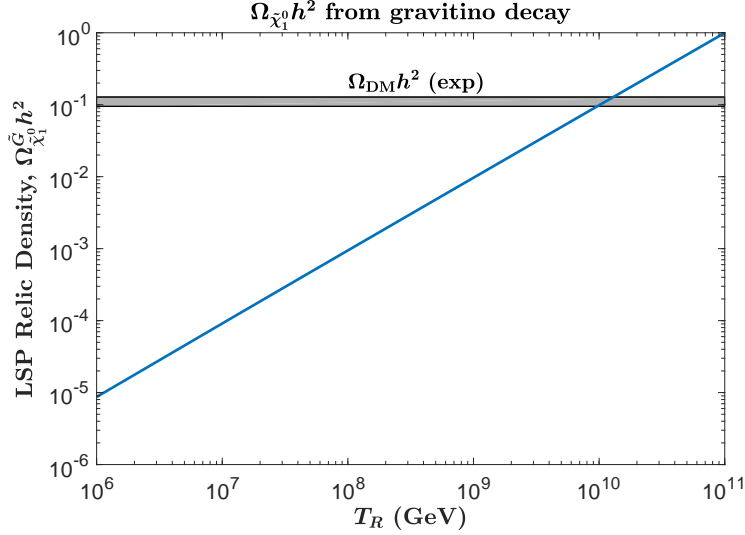


Figure 2: Neutralino relic density arising from the decay of thermally produced gravitinos vs the reheating temperature using the model points of Table 1. All the model points lie on the thin blue line. The squeezing of the model points on to the thin blue line arises because for $m_i^2/m_{\tilde{G}}^2 \ll 1$ the gravitino production is dominated by $\pm 3/2$ helicity states while the production of $\pm 1/2$ helicity states is suppressed by a factor $(m_i^2/m_{\tilde{G}}^2)$ (see Eq. 18). The grey patch corresponds to $\Omega_{DM} h^2$ (exp), the experimental limits on dark matter relics from the WMAP and PLANCK experiments.

becomes independent of the gravitino mass in the limit $m_i/m_{\tilde{G}} \ll 1$ which is the case for the model points of Table 1. The analysis of Fig 2 shows that the neutralino relic density arising from gravitino decay is below the relic density given by WMAP and PLANCK up to reheating temperature of 10^{10} GeV and is a negligible fraction of the total for reheating temperatures below 10^9 GeV. The deduction of the reheating temperature is rather model dependent since it involves the nature of the inflaton, its coupling to the standard model fields and the possible modes of its decay, i.e., gauge, Yukawa or gravitational. Thus the analysis presented above is in terms of the reheating temperature rather than in terms of an underlying inflaton model.

7 Dark matter in SUGRA with 50-100 TeV scalars

The analysis presented in Table 12 gives us a set of models which are consistent with the Higgs boson mass constraint and the relic density consistent with the WMAP and PLANCK experiments and would be discoverable at the LHC with an integrated luminosity well below the optimal integrated luminosity achievable at the LHC. It is also of interest to investigate if some or all of these models are discoverable in direct detection experiment. The direct detection of the neutralinos depends crucially on its gaugino-higgsino content. Thus the neutralino is a linear combination of four states $\tilde{\chi}^0 = \alpha\lambda^0 + \beta\lambda^3 + \gamma\tilde{H}_1 + \delta\tilde{H}_2$ where λ^0, λ^3 are the bino, wino and \tilde{H}_1, \tilde{H}_2 are the higgsinos. For the models of Table 1, $|\beta| \leq 0.324, |\gamma| \leq 0.003, |\delta| = 0.000$. One finds that the wino and the higgsino content of the models of Table 1

are small, and the neutralino is essentially a bino. The fact that the neutralino is mostly a bino makes the neutralino-proton cross section relatively small. In Table 15 we present the spin independent and spin-dependent neutralino-proton cross sections for these models. The analysis of Table 15 shows that the spin-independent neutralino-proton cross section is $\mathcal{O}(10^{-48}\text{cm}^{-2})$, and only three out of the ten benchmarks lie above the neutrino floor [91] which is the threshold for detectability (see Fig. 10). Those points would thus be out of reach of the future dark matter experiments LUX-ZEPLIN [92, 93]. However, as Table 12 shows they would be discoverable at the LHC.

8 Conclusions

Supersymmetry is desirable for a number of theoretical as well as phenomenological reasons. Supergravity unification provides a framework with a small number of parameters at a high scale in terms of which the properties of low energy effective theory can be computed. Supergravity unified models also accomplish radiative breaking of the electroweak symmetry which allows a determination of the sparticle mass spectrum with the given high scale input and thus determines the weak SUSY scale. The observation of the Higgs boson mass at ~ 125 GeV implies that the loop correction to the tree level Higgs boson mass is large which in turn implies that the scale of weak scale supersymmetry lies in the several TeV region. This makes the search for supersymmetry more challenging than initially thought. For high scale models, there is another aspect which makes the observation of supersymmetry challenging. This concerns dark matter. Thus for high scale models one finds that often the parameter space that gives the desired Higgs boson mass gives a neutralino which is mostly a bino. For a bino type neutralino, one needs coannihilation to achieve the appropriate relic density consistent with the WMAP and PLANCK experiments. This means that there must be one or more sparticles close by to coannihilate with the neutralino. The relatively small mass gap between the neutralino and the coannihilating particles implies that the final states in the decay of the coannihilation process would be soft and thus hard to detect.

In this analysis we have investigated high scale models with scalars in the mass range 50-100 TeV while the gauginos are relatively light. Scalar masses in the assumed range are interesting as they alleviate a number of problems associated with low weak SUSY scale. One such problem concerns the SUSY CP problem which leads to large EDMs for leptons and quarks significantly above the existing experimental limits. Aside from fine tuning the CP phases to be extremely small, the other options include mass suppression [94] or the cancellation mechanism [95]. The models with scalar masses in the 50-100 TeV naturally provide a large mass suppression of the EDMs alleviating this problem in a significant way. Another problem of low weak SUSY scale concerns rapid proton decay even with R-parity conservation due to baryon and lepton number violating dimension five operators. Again scalar masses in the 50-100 TeV range resolve this problem in a natural way [29]. In the analysis presented here we created a number of benchmark models consistent with radiative electroweak symmetry breaking, Higgs boson mass constraint and the relic density constraint on neutralino dark matter. We used an extensive set of signal regions and optimized them for the model points we discuss. In the analysis we found a number of signatures with 0,

1 and 2 leptons, 2 and 4 jets, along with other kinematical constraints which allow a 5σ discovery for some of our benchmarks with an integrated luminosity of 100 fb^{-1} . All of the remaining benchmarks are found to be discoverable with an integrated luminosity of 1000 fb^{-1} which is significantly below the optimum integrated luminosity that can be reached in the high luminosity era of the LHC.

We also investigated the influence of 50-100 TeV scalar masses on unification of gauge coupling constants. It is found that unification of the gauge couplings using LEP data occurs with the same degree of accuracy as for the case with weak scale supersymmetry in the TeV region. Further, we analyzed the decay of the gravitinos in this model and found that the gravitinos decay before the time scale $(1 - 10^2)\text{s}$ and do not upset the BBN. Further, we analyzed the thermal production of gravitinos and their contribution to the non-thermal relic density of the neutralinos. Here one finds that this contribution is negligible up to reheat temperature of 10^9 GeV . We also analyzed the spin-independent neutralino-proton cross section. It is found that only few of those points have cross sections lying above the neutrino floor while others are below it making them difficult to detect even with future dark matter experiments such as LUX, ZEPLIN and XENON1T. Thus the latter set could only be discovered at the LHC. In summary, high scale models with scalar masses lying in the 50-100 TeV have the possibility of being discovered at the LHC and such models also have several redeeming properties as they alleviate some of the problems encountered by low weak scale SUSY models.

Finally we note the analysis above exhibits the remarkable effect of dark matter constraints through coannihilation on limiting the parameter space of models and thus controlling the discovery potential of the LHC for supersymmetry. One can thus expect some influence on the LHC analyses if the nature of dark matter was not pure neutralino but was multi-component (see e.g., [96]). One such possibility proposed recently is in the form of an ultralight axion[97]. If this were the case the relic density arising from neutralino would decrease making the dark matter constraint on the analysis more stringent. However, at this time there is no compelling evidence for the multicomponent nature of dark matter.

Acknowledgments: Correspondences with Howard Baer and Tom Cridge are acknowledged. The analysis presented here was done using the resources of the high-performance Cluster353 at the Advanced Scientific Computing Initiative (ASCI) at Northeastern University. This research was supported in part by the NSF Grant PHY-1620575.

9 Tables

Model	m_0	A_0	m_1	m_2	m_3	$\tan \beta$
(a)	70760	141410	544	481	983	45
(b)	77710	155593	503	426	1645	11
(c)	92390	183892	557	474	1441	18
(d)	82900	165862	539	466	1275	6
(e)	63057	126110	504	414	1472	28
(f)	67248	134496	543	446	1482	30
(g)	54981	109990	521	419	1388	34
(h)	86618	172526	610	497	1369	23
(i)	58619	117055	550	425	1204	25
(j)	74199	148386	620	487	1000	27

Table 1: Input parameters for benchmarks for high weak scale supergravity models with m_0 in the range 50 – 100 TeV range. All masses are in GeV.

Model	h^0	$\tilde{\mu}$	$\tilde{\chi}_1^0$	$\tilde{\chi}_1^\pm$	\tilde{t}	\tilde{g}	$m_{\tilde{q}}$	$m_{\tilde{f}}$	$\Omega_{\tilde{\chi}_1^0}^{\text{th}} h^2$
(a)	124.9	21006	114.1	134.2	36219	2149	70362	63300	0.103
(b)	125.5	30025	129.2	144.5	37578	3799	77314	73600	0.108
(c)	124.4	31386	130.0	145.9	46109	3336	91885	87000	0.126
(d)	124.8	34655	136.1	152.5	40236	2922	82456	78700	0.126
(e)	124.9	23457	136.2	156.0	30474	3403	62740	58500	0.113
(f)	123.6	24163	147.3	169.4	32873	3405	66909	62200	0.127
(g)	123.2	20755	147.7	170.6	26391	3211	54707	50400	0.115
(h)	126.7	27898	169.4	192.5	43771	3106	86200	81200	0.115
(i)	123.7	21964	170.9	195.3	28254	2795	58300	54700	0.114
(j)	124.3	24222	187.1	214.9	37276	2252	73800	69100	0.085

Table 2: The Higgs boson (h^0) mass, some relevant sparticle masses, and the relic density for the benchmarks of Table 1. Here $m_{\tilde{q}}$ stands for the mass of the heaviest squark and $m_{\tilde{f}}$ for the average sfermion mass. All masses are in GeV.

Model	full SUSY	$qq \rightarrow \tilde{\chi}_2^0 \tilde{\chi}_1^\pm$	$qq \rightarrow \tilde{\chi}_1^+ \tilde{\chi}_1^-$	$qq \rightarrow \tilde{\chi}_1^0 \tilde{\chi}_1^\pm$	$qq \rightarrow \tilde{g} \tilde{g}$	$gg \rightarrow \tilde{g} \tilde{g}$
(a)	9.45	5.82	3.08	0.55	2.4×10^{-4}	1.7×10^{-4}
(b)	7.16	4.79	2.37	3.7×10^{-5}	1.9×10^{-7}	1.3×10^{-8}
(c)	6.92	4.63	2.29	1.3×10^{-4}	1.3×10^{-6}	2.1×10^{-7}
(d)	5.91	3.96	1.95	8.7×10^{-6}	7.9×10^{-6}	2.3×10^{-6}
(e)	5.50	3.47	1.80	0.22	9.8×10^{-7}	1.4×10^{-7}
(f)	4.10	2.57	1.34	0.19	9.7×10^{-7}	1.4×10^{-7}
(g)	4.00	2.48	1.30	0.22	2.2×10^{-6}	4.4×10^{-7}
(h)	2.58	1.62	0.84	0.12	3.6×10^{-6}	7.8×10^{-7}
(i)	2.46	1.52	0.80	0.14	1.4×10^{-5}	4.6×10^{-6}
(j)	1.74	1.03	0.56	0.15	1.5×10^{-4}	9.6×10^{-5}

Table 3: SUSY production cross sections, in pico-barns, for benchmarks of Table 1 where “full SUSY” stands for the total production cross section including all the sparticle final states in the production.

Model	$\tilde{\chi}_2^0 \rightarrow \tilde{\chi}_1^0 q \bar{q}$ $q \in \{u, d, c, s, b\}$	$\tilde{\chi}_2^0 \rightarrow \tilde{\chi}_1^0 \ell \bar{\ell}$ $\ell \in \{e, \mu, \tau, \nu\}$	$\tilde{g} \rightarrow \tilde{\chi}_1^0 q \bar{q}$ $q \in \{u, d, c, s, t, b\}$	$\tilde{g} \rightarrow \tilde{\chi}_2^0 q \bar{q}$	$\tilde{g} \rightarrow \tilde{\chi}_1^\pm q_i \bar{q}_j$
(a)	0.73	0.27	0.18	0.27	0.55
(b)	0.71	0.29	0.28	0.24	0.48
(c)	0.72	0.28	0.25	0.25	0.50
(d)	0.66	0.34	0.28	0.24	0.48
(e)	0.76	0.24	0.25	0.25	0.50
(f)	0.76	0.24	0.24	0.25	0.51
(g)	0.77	0.23	0.24	0.25	0.51
(h)	0.74	0.26	0.24	0.25	0.51
(i)	0.76	0.24	0.26	0.25	0.49
(j)	0.75	0.25	0.23	0.25	0.52

Table 4: Branching ratios for dominant decays of $\tilde{\chi}_2^0$ and \tilde{g} for benchmarks of Table 1 where $q_i \bar{q}_j = \{(u\bar{d}), (d\bar{u}), (s\bar{c}), (c\bar{s}), (b\bar{t}), (t\bar{b})\}$.

Model	$\tilde{\chi}_1^\pm \rightarrow \tilde{\chi}_1^0 q_i \bar{q}_j$ $q \in \{u, d, c, s\}$	$\tilde{\chi}_1^\pm \rightarrow \tilde{\chi}_1^0 \ell^\pm \nu_\ell$ $\ell \in \{e, \mu, \tau\}$
(a)	0.67	0.33
(b)	0.67	0.33
(c)	0.67	0.33
(d)	0.67	0.33
(e)	0.67	0.33
(f)	0.67	0.33
(g)	0.67	0.33
(h)	0.67	0.33
(i)	0.67	0.33
(j)	0.67	0.33

Table 5: Branching ratios for dominant decays of $\tilde{\chi}_1^\pm$ for benchmarks of Table 1 where $q_i \bar{q}_j = \{(u\bar{d}), (c\bar{s}), (t\bar{b})\}$.

Requirement	$0\ell nj$					
	$0\ell 2j\text{-A}$	$0\ell 2j\text{-B}$	$0\ell 2j\text{-C}$	$0\ell 4j\text{-A}$	$0\ell 4j\text{-B}$	$0\ell 4j\text{-C}$
$N(\text{jets})$	≥ 2	≥ 2	≥ 2	≥ 4	≥ 4	≥ 4
$p_T(j_1)$ (GeV) <	100	100	100	100	100	100
$p_T(j_2)$ (GeV) <	60	60	60	80	80	80
$p_T(j_4)$ (GeV) <				50	50	50
E_T^{miss} (GeV) <	250	250	250	400	400	400
$\Delta\phi(\text{jet}_1, E_T^{\text{miss}})$ (rad) >	1.5	1.5	1.5	2.5	2.5	2.5
$\min[\Delta\phi(\text{jet}_{1-2}, E_T^{\text{miss}})]$ (rad) <	2.5	2.5	2.5			
m_{T2} (GeV) >	100	100	100			
m_{T2} (GeV) <	400	400	400			
m_{jj} (GeV) >	50	50	50			
m_{jj} (GeV) <	700	700	700			
$m_T^{\min}(\text{jet}_{1-2}, E_T^{\text{miss}})$ (GeV) <				120	120	120
m_{eff} (GeV) >				250	250	250
m_{eff} (GeV) <				350	350	350
$E_T^{\text{miss}}/\sqrt{H_T}(\text{GeV}^{1/2})$ >	1	1	1			
$E_T^{\text{miss}}/\sqrt{H_T}(\text{GeV}^{1/2})$ <	15	15	13			
H_T (GeV) <	115	120	120	155	160	165

Table 6: The selection criteria ($0\ell nj$) used for the signal regions implies that the signal consists of zero leptons (veto on electrons and muons) and n jets where n is a minimum of 2 or 4 jets in the final state. The blank spaces indicate that the kinematical variable is either not applicable to the corresponding SR or has not been used.

Model	\mathcal{L} for 5σ discovery in $0\ell nj$					
	$0\ell 2j$ -A	$0\ell 2j$ -B	$0\ell 2j$ -C	$0\ell 4j$ -A	$0\ell 4j$ -B	$0\ell 4j$ -C
(a)	86	431	492	100	422	417
(b)	150	920	990	175	734	1290
(c)	114	1060	1140	749
(d)	174	864	864			
(e)	83	848	894	74	199	548
(f)	173	1250	1450	534	560	1420
(g)	196	1250	1250	63	147	460
(h)	558	2870	3000	337	905	1830
(i)	1120	1480	1560	2010
(j)	771	2960

Table 7: Analysis of the discovery potential for supersymmetry for the parameter set of Table 1, using the selection criteria of Table 6, where the minimum integrated luminosity needed for 5σ discovery is given in fb^{-1} . Here and in the tables following ... indicates that the minimum integrated luminosity needed for 5σ discovery exceeds 3000 fb^{-1} . Blank spaces mean that zero events passed the cuts.

Requirement	$1\ell 2j$		
	$1\ell 2j$ -A	$1\ell 2j$ -B	$1\ell 2j$ -C
$N(\text{jets})$	≥ 2	≥ 2	≥ 2
$p_T(j_1) \text{ (GeV)} <$	60	70	80
$p_T(j_2) \text{ (GeV)} <$	50	50	50
Leading $p_T^\ell \text{ (GeV)} >$	10	10	10
Leading $p_T^\ell \text{ (GeV)} <$	40	40	40
$m_T^\ell \text{ (GeV)} <$	60	60	60
$m_T^{\text{min}}(\text{jet}_{1-2}, E_T^{\text{miss}}) \text{ (GeV)} <$	140	140	140
$m_{\text{eff}} \text{ (GeV)} >$	180	180	180
$m_{\text{eff}} \text{ (GeV)} <$	240	240	240
$E_T^{\text{miss}} \text{ (GeV)} <$	250	250	250
$\Delta\phi(\text{jet}_1, E_T^{\text{miss}}) \text{ (rad)} >$	2.5	2.5	2.5
$H_T \text{ (GeV)} <$	105	105	105

Table 8: The selection criteria ($1\ell 2j$) used for the signal regions corresponding to a single lepton, missing transverse energy and a minimum of 2 jets in the final state.

	\mathcal{L} for 5σ discovery in 1L2J		
Model	1 ℓ 2 j -A	1 ℓ 2 j -B	1 ℓ 2 j -C
(a)	1200	221	80
(b)	520	385	217
(c)	2230	...	928
(f)	2640
(g)	1670	2780	2780
(h)	...	1670	1070

Table 9: Analysis of the discovery potential for supersymmetry for the parameter space of Table 1, using the selection criteria of Table 8, where the minimum integrated luminosity needed for 5σ discovery is given in fb^{-1} . Points (d), (e), (i) and (j) are not displayed since the minimum integrated luminosity needed for their discovery exceeds 3000 fb^{-1} for this signal region.

Requirement	2 ℓ 1 j -SF			2 ℓ 1 j -DF		
	2 ℓ 1 j -SF-A	2 ℓ 1 j -SF-B	2 ℓ 1 j -SF-C	2 ℓ 1 j -DF-A	2 ℓ 1 j -DF-B	2 ℓ 1 j -DF-C
E_T^{miss} (GeV) <	150	150	150	150	150	150
m_T^ℓ (GeV) <	80	80	80	80	80	80
$\Delta\phi(j_1, E_T^{\text{miss}})$ (rad) >	2.7	2.7	2.7	2.7	2.7	2.7
$\Delta R_{\ell\ell}$ (rad) <	1.0	1.0	1.0	3.0	3.0	3.0
$m_{\ell\ell}$ (GeV) <	50	50	50	40	40	40
E_T^{miss}/H_T >	0.7	0.7	0.7	0.7	0.7	0.7
m_{eff} (GeV) >	160	160	160	160	160	160
m_{eff} (GeV) <	260	270	280	260	270	280

Table 10: The selection criteria used for the signal regions related to the 2 lepton signature. Here and in the tables following SF stands for same flavor opposite sign lepton pair and DF stands for different flavor opposite sign lepton pair.

Model	\mathcal{L} for 5σ discovery in $2\ell 1j$ -SF		
	$2\ell 1j$ -SF-A	$2\ell 1j$ -SF-B	$2\ell 1j$ -SF-C
(a)	131	167	214
(b)	228	291	93
(c)	975	1250	1590
(d)	334	427	243
(e)	172	219	281
(f)	309	222	126
(g)	729	932	530
(h)	1750	560	716
(i)	857	616	504
(j)	...	2190	2800

Table 11: Analysis of the discovery potential for supersymmetry for the parameter space of Table 1, using the 2 lepton same flavor (SF) selection criteria of Table 10, where the minimum integrated luminosity needed for 5σ discovery is given in fb^{-1} . Results from the different flavor (DF) SR are not displayed because of their poor performance.

Model	Leading SR	\mathcal{L} (fb^{-1})	Sub-leading SR	\mathcal{L} (fb^{-1})
(g)	$0\ell 4j$ -A	63 ± 8	$0\ell 4j$ -B	147 ± 19
(e)	$0\ell 4j$ -A	74 ± 10	$0\ell 2j$ -A	83 ± 9
(a)	$1\ell 2j$ -C	80 ± 9	$0\ell 2j$ -A	86 ± 9
(b)	$2\ell 1j$ -SF-C	93 ± 16	$0\ell 2j$ -A	150 ± 17
(c)	$0\ell 2j$ -A	114 ± 13	$0\ell 4j$ -A	749 ± 84
(f)	$2\ell 1j$ -SF-C	126 ± 22	$0\ell 2j$ -A	173 ± 19
(d)	$0\ell 2j$ -A	174 ± 19	$2\ell 1j$ -SF-C	243 ± 43
(h)	$0\ell 4j$ -A	337 ± 44	$0\ell 2j$ -A	558 ± 63
(i)	$2\ell 1j$ -SF-C	504 ± 89	$2\ell 1j$ -SF-B	616 ± 109
(j)	$0\ell 2j$ -A	771 ± 87	$2\ell 1j$ -SF-B	2190 ± 387

Table 12: The overall minimum integrated luminosities needed for 5σ discovery using the leading and the sub-leading signal regions for benchmarks of Table 1, including all signal regions discussed. The estimated uncertainties in the predicted integrated luminosities are shown. The third column shows that all the benchmark can be discovered with an integrated luminosity below 1000 fb^{-1} which is significantly below the optimum integrated luminosity achievable at the LHC.

Signal Region	Signal systematics	Background systematics
$0\ell 2j$	12.8%	19.1%
$0\ell 4j$	18.3%	23.1%
$1\ell 2j$	13.2%	19.4%
$2\ell 1j$ -SF	28.1%	31.4%

Table 13: Total estimated systematic uncertainties on signal and background for the four leading signal regions.

Model	$\text{Br}(\tilde{G} \rightarrow \tilde{g}g)$	$\text{Br}(\tilde{G} \rightarrow \tilde{\chi}_1^\pm W^\mp)$	$\text{Br}(\tilde{G} \rightarrow \tilde{\chi}_1^0 \gamma)$	$\text{Br}(\tilde{G} \rightarrow \tilde{\chi}_1^0 Z)$	$\Gamma_{\tilde{G}}^{\text{two-body}} \times 10^{-24}$ (GeV)	Lifetime (s)
(a)	0.598	0.150	0.040	0.035	7.9	0.083
(b)	0.619	0.156	0.060	0.018	10.1	0.065
(c)	0.619	0.155	0.058	0.020	17.0	0.039
(d)	0.620	0.156	0.057	0.021	12.3	0.053
(e)	0.616	0.155	0.044	0.033	5.4	0.121
(f)	0.616	0.155	0.043	0.034	6.6	0.099
(g)	0.614	0.155	0.041	0.036	3.6	0.183
(h)	0.618	0.155	0.038	0.039	14.1	0.047
(i)	0.617	0.155	0.041	0.037	4.4	0.151
(j)	0.617	0.155	0.036	0.042	8.9	0.074

Table 14: Branching ratios of the leading decay channels of the gravitino, the total two-body decay width and the lifetime of the gravitino for the benchmarks of Table 1.

Model	$\sigma_{p,\chi_1^0}^{\text{SI}} \times 10^{49}$	$\sigma_{p,\chi_1^0}^{\text{SD}} \times 10^{47}$
(a)	25.4	3.01
(b)	12.9	63.8
(c)	37.7	68.2
(d)	5.52	133
(e)	15.1	5.83
(f)	16.4	6.10
(g)	13.5	3.06
(h)	13.9	10.2
(i)	8.26	3.71
(j)	9.20	4.13

Table 15: Proton-neutralino spin-independent ($\sigma_{p,\chi_1^0}^{\text{SI}}$) and spin-dependent ($\sigma_{p,\chi_1^0}^{\text{SD}}$) cross-sections in units of cm^{-2} for the benchmarks of Table 1.

10 Figures

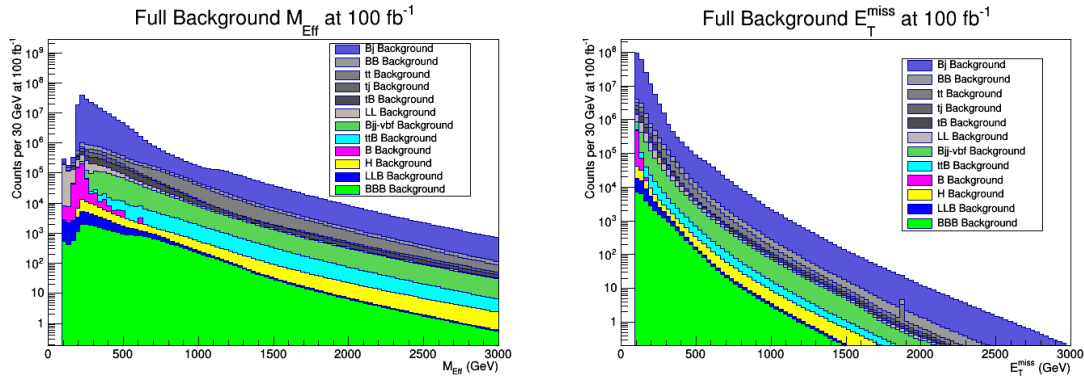


Figure 3: Full SNOWMASS standard model background [51] after triggering cuts and a cut of $E_T^{\text{miss}} \geq 100$ GeV, broken into final states and scaled to 100 fb^{-1} . The left panel gives $M_{\text{eff}}(\text{incl.})$ and the right panel gives E_T^{miss} . Individual data sets are labeled according to Eq. 1.

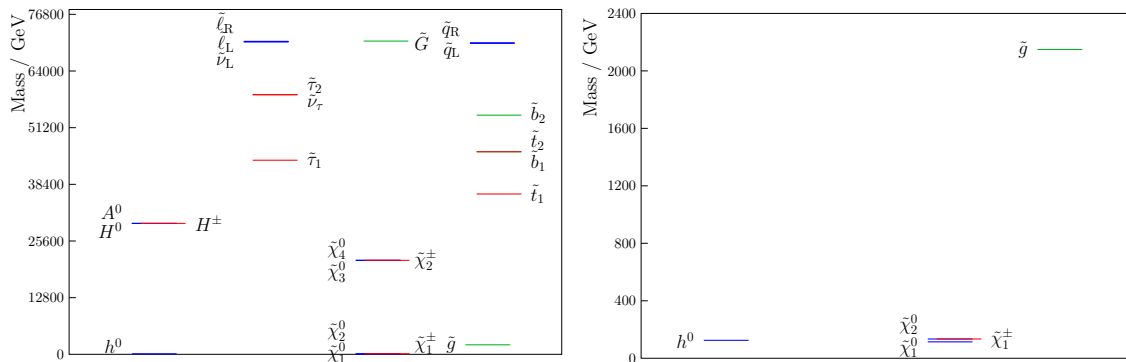


Figure 4: The sparticle spectrum for the benchmark (a) of Table 1. The figure in the left panel shows the entire spectrum with the heavy sfermions having mass at the order of m_0 . The right panel shows the light spectrum which consists of the Higgs boson and the gauginos $\tilde{\chi}_1^0, \tilde{\chi}_2^0, \tilde{\chi}_1^\pm$ and \tilde{g} .

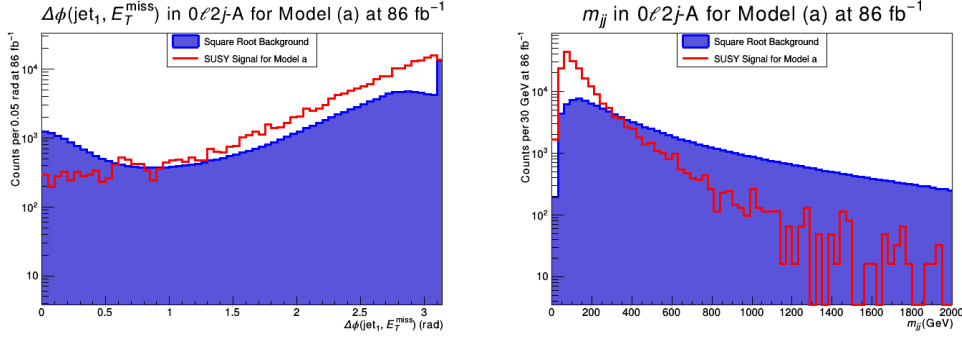


Figure 5: Left panel: Distribution in $\Delta\phi(\text{jet}_1, E_T^{\text{miss}})$ for the $0\ell 2j\text{-A}$ signal region defined in Table 6 for the benchmark (a) of Table 1. Plotted is the number of counts for the SUSY signal per 0.05 rad and the square root of the total standard model SNOWMASS background. The analysis is done at 86 fb^{-1} of integrated luminosity, which gives a 5σ discovery in this signal region. Right panel: Distribution in the dijet invariant mass m_{jj} where number of counts per 30 GeV is plotted for the same point as in the left panel.

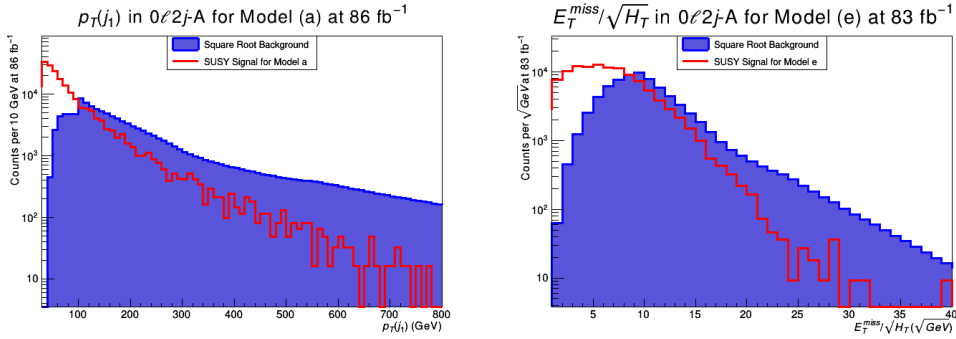


Figure 6: Left panel: Distribution in $p_T(j_1)$ for the $0\ell 2j\text{-A}$ signal region defined in Table 6 for benchmark (a) of Table 1. Plotted is the number of counts for the SUSY signal per 10 GeV and the square root of the total standard model SNOWMASS background. The analysis is done at 86 fb^{-1} of integrated luminosity, which gives a 5σ discovery in this signal region. Right panel: Distribution in the variable $E_T^{\text{miss}}/\sqrt{H_T}$ where number of counts per $\sqrt{\text{GeV}}$ is plotted for benchmark (e) of Table 1 at 83 fb^{-1} .

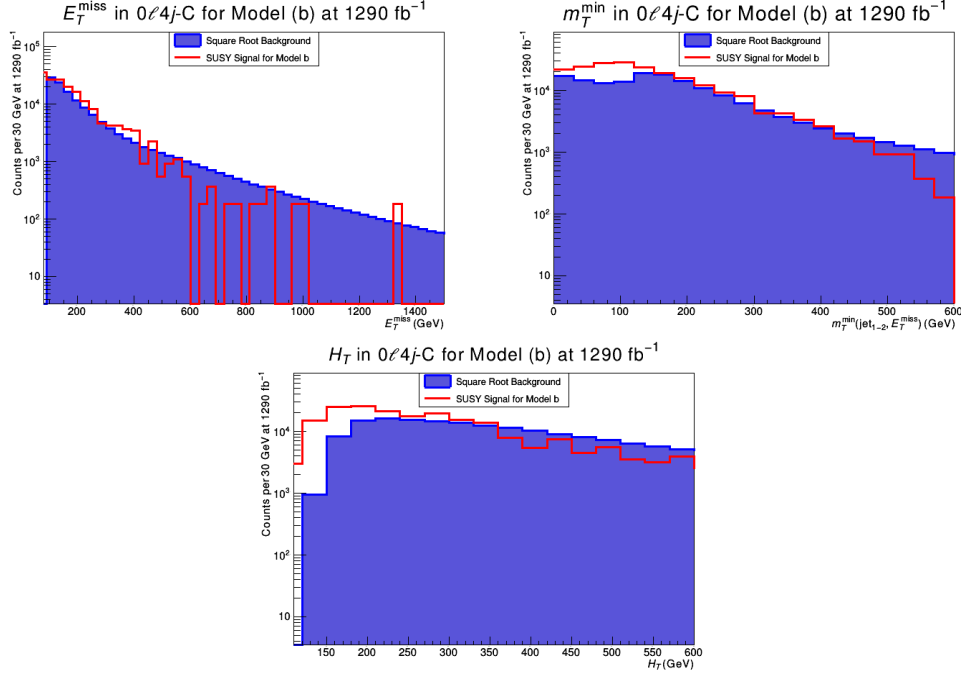


Figure 7: Top left panel: Distribution in E_T^{miss} for the $0\ell 4j\text{-C}$ signal region defined in Table 6 for benchmark (b) of Table 1. Plotted is the number of counts for the SUSY signal per 30 GeV and the square root of the total standard model SNOWMASS background. The analysis is done at 1290 fb⁻¹ of integrated luminosity, which gives a 5σ discovery in this signal region. Top right panel: Same analysis as in adjacent panel but for the distribution in $m_T^{\text{min}}(\text{jet}_{1-2}, E_T^{\text{miss}})$. Bottom panel: Same analysis as in the top panels but for the distribution in H_T .

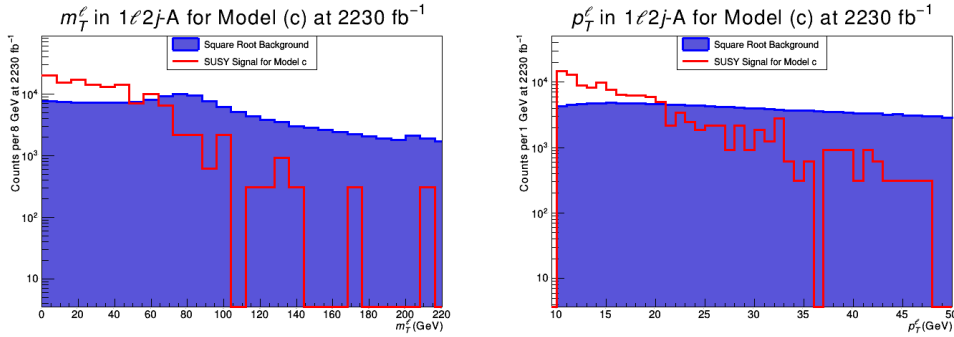


Figure 8: Left panel: Distribution in m_T^ℓ for the $1\ell 2j\text{-A}$ signal region defined in Table 8 for benchmark (c) of Table 1. Plotted is the number of counts for the SUSY signal per 8 GeV and the square root of the total standard model SNOWMASS background. The analysis is done at 2230 fb⁻¹ of integrated luminosity, which gives a 5σ discovery in this signal region. Right panel: same analysis as in the left panel but for the distribution in p_T^ℓ .

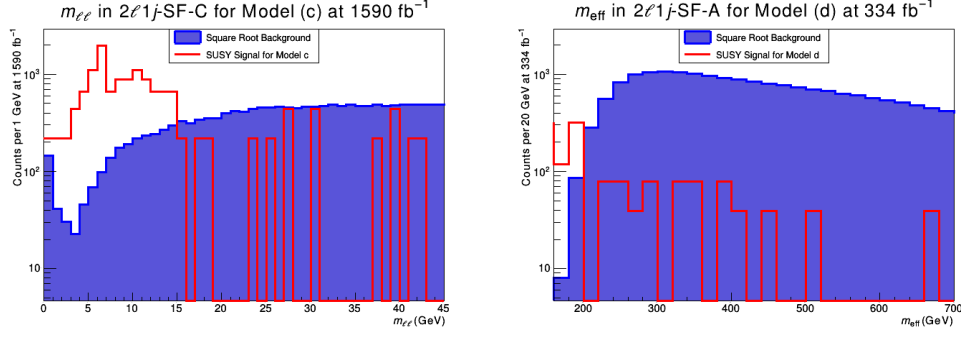


Figure 9: Left panel: Distribution in the dilepton invariant mass, $m_{\ell\ell}$, for the $2\ell 1j$ -SF-C signal region defined in Table 10 for benchmark (c) of Table 1. Plotted is the number of counts for the SUSY signal per GeV and the square root of the total standard model SNOWMASS background. The analysis is done at 1590 fb^{-1} of integrated luminosity, which gives a 5σ discovery in this signal region. Right panel: Distribution in m_{eff} for the $2\ell 1j$ -SF-A signal region defined in Table 10 for benchmark (d) of Table 1. Plotted is the number of counts for the SUSY signal per 20 GeV and the square root of the total standard model SNOWMASS background. The analysis is done at 334 fb^{-1} of integrated luminosity

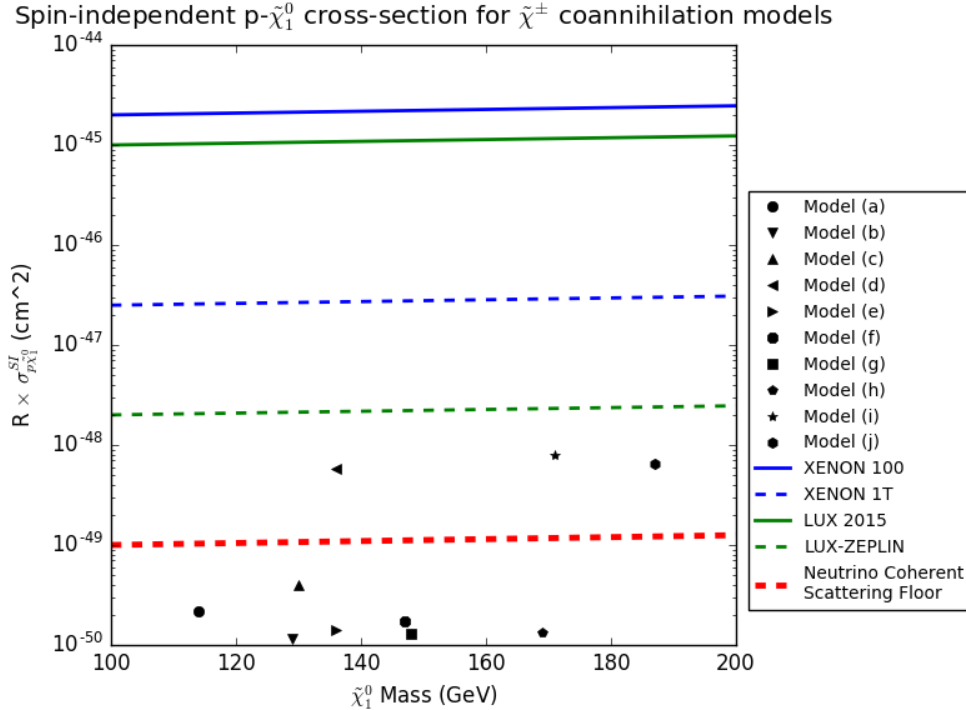


Figure 10: $R \times \sigma_{p, \tilde{\chi}_1^0}^{\text{SI}}$ ($R = \rho_{\tilde{\chi}_1^0}/\rho_c$) for benchmarks of Table 1 as a function of LSP mass displayed alongside the current and projected range of the XENON and LUX experiments and the neutrino floor [93].

References

- [1] F. Englert and R. Brout, Phys. Rev. Lett. **13**, 321 (1964). doi:10.1103/PhysRevLett.13.321
- [2] P. W. Higgs, Phys. Rev. Lett. **13**, 508 (1964). doi:10.1103/PhysRevLett.13.508
- [3] G. S. Guralnik, C. R. Hagen and T. W. B. Kibble, Phys. Rev. Lett. **13**, 585 (1964). doi:10.1103/PhysRevLett.13.585
- [4] S. Chatrchyan *et al.* [CMS Collaboration], Phys. Lett. B **716**, 30 (2012) doi:10.1016/j.physletb.2012.08.021 [arXiv:1207.7235 [hep-ex]].
- [5] G. Aad *et al.* [ATLAS Collaboration], Phys. Lett. B **716**, 1 (2012) doi:10.1016/j.physletb.2012.08.020 [arXiv:1207.7214 [hep-ex]].
- [6] A. H. Chamseddine, R. Arnowitt and P. Nath, Phys. Rev. Lett. **49** (1982) 970; P. Nath, R. L. Arnowitt and A. H. Chamseddine, Nucl. Phys. B **227**, 121 (1983); L. J. Hall, J. D. Lykken and S. Weinberg, Phys. Rev. D **27**, 2359 (1983). doi:10.1103/PhysRevD.27.2359
- [7] P. Nath, “Supersymmetry, Supergravity, and Unification”, Cambridge University Press. ISBN: 9780521197021 (2016).
- [8] S. Akula, B. Altunkaynak, D. Feldman, P. Nath and G. Peim, Phys. Rev. D **85**, 075001 (2012) doi:10.1103/PhysRevD.85.075001 [arXiv:1112.3645 [hep-ph]].
- [9] A. Arbey, M. Battaglia, A. Djouadi and F. Mahmoudi, JHEP **1209**, 107 (2012) doi:10.1007/JHEP09(2012)107 [arXiv:1207.1348 [hep-ph]].
- [10] H. Baer, V. Barger and A. Mustafayev, Phys. Rev. D **85**, 075010 (2012) doi:10.1103/PhysRevD.85.075010 [arXiv:1112.3017 [hep-ph]]; A. Arbey, M. Battaglia, A. Djouadi, F. Mahmoudi and J. Quevillon, Phys. Lett. B **708**, 162 (2012) doi:10.1016/j.physletb.2012.01.053 [arXiv:1112.3028 [hep-ph]]; P. Draper, P. Meade, M. Reece and D. Shih, Phys. Rev. D **85**, 095007 (2012) doi:10.1103/PhysRevD.85.095007 [arXiv:1112.3068 [hep-ph]]. M. Carena, S. Gori, N. R. Shah and C. E. M. Wagner, JHEP **1203**, 014 (2012) doi:10.1007/JHEP03(2012)014 [arXiv:1112.3336 [hep-ph]]; O. Buchmueller *et al.*, Eur. Phys. J. C **72**, 2020 (2012) doi:10.1140/epjc/s10052-012-2020-3 [arXiv:1112.3564 [hep-ph]]; S. Akula, P. Nath and G. Peim, Phys. Lett. B **717**, 188 (2012) doi:10.1016/j.physletb.2012.09.007 [arXiv:1207.1839 [hep-ph]]. C. Strey, G. Bertone, F. Feroz, M. Fornasa, R. Ruiz de Austri and R. Trotta, JCAP **1304**, 013 (2013) doi:10.1088/1475-7516/2013/04/013 [arXiv:1212.2636 [hep-ph]].
- [11] H. Baer, V. Barger and M. Savoy, Phys. Scripta **90**, 068003 (2015) doi:10.1088/0031-8949/90/6/068003 [arXiv:1502.04127 [hep-ph]].
- [12] R. L. Arnowitt and P. Nath, Phys. Rev. Lett. **69**, 725 (1992). doi:10.1103/PhysRevLett.69.725

- [13] D. Larson *et al.*, *Astrophys. J. Suppl.* **192**, 16 (2011) doi:10.1088/0067-0049/192/2/16 [arXiv:1001.4635 [astro-ph.CO]].
- [14] P. A. R. Ade *et al.* [Planck Collaboration], *Astron. Astrophys.* **594**, A13 (2016) doi:10.1051/0004-6361/201525830 [arXiv:1502.01589 [astro-ph.CO]].
- [15] K. Griest and D. Seckel, *Phys. Rev. D* **43**, 3191 (1991). doi:10.1103/PhysRevD.43.3191
- [16] D. Feldman, Z. Liu and P. Nath, *Phys. Rev. Lett.* **99**, 251802 (2007) Erratum: [*Phys. Rev. Lett.* **100**, 069902 (2008)] doi:10.1103/PhysRevLett.99.251802 [arXiv:0707.1873 [hep-ph]]; *Phys. Lett. B* **662**, 190 (2008); *JHEP* **0804**, 054 (2008); N. Chen, D. Feldman, Z. Liu, P. Nath and G. Peim, *Phys. Rev. D* **83**, 035005 (2011) doi:10.1103/PhysRevD.83.035005 [arXiv:1011.1246 [hep-ph]]; D. Francescone, S. Akula, B. Altunkaynak and P. Nath, *JHEP* **1501**, 158 (2015) doi:10.1007/JHEP01(2015)158 [arXiv:1410.4999 [hep-ph]].
- [17] J. R. Ellis, K. Enqvist, D. V. Nanopoulos and K. Tamvakis, *Phys. Lett.* **155B**, 381 (1985). doi:10.1016/0370-2693(85)91591-6
- [18] A. Corsetti and P. Nath, *Phys. Rev. D* **64**, 125010 (2001); U. Chattopadhyay and P. Nath, *Phys. Rev. D* **65**, 075009 (2002); A. Birkedal-Hansen and B. D. Nelson, *Phys. Rev. D* **67**, 095006 (2003); U. Chattopadhyay and D. P. Roy, *Phys. Rev. D* **68**, 033010 (2003); D. G. Cerdeno and C. Munoz, *JHEP* **0410**, 015 (2004); G. Belanger, F. Boudjema, A. Cottrant, A. Pukhov and A. Semenov, *Nucl. Phys. B* **706**, 411 (2005); H. Baer, A. Mustafayev, E. K. Park, S. Profumo and X. Tata, *JHEP* **0604**, 041 (2006); K. Choi and H. P. Nilles *JHEP* **0704** (2007) 006; I. Gogoladze, R. Khalid, N. Okada and Q. Shafi, arXiv:0811.1187 [hep-ph]; I. Gogoladze, F. Nasir, Q. Shafi and C. S. Un, *Phys. Rev. D* **90**, no. 3, 035008 (2014) doi:10.1103/PhysRevD.90.035008 [arXiv:1403.2337 [hep-ph]]; S. Bhattacharya, A. Datta and B. Mukhopadhyaya, *Phys. Rev. D* **78**, 115018 (2008); M. E. Gomez, S. Lola, P. Naranjo and J. Rodriguez-Quintero, arXiv:0901.4013 [hep-ph]; B. Altunkaynak, P. Grajek, M. Holmes, G. Kane and B. D. Nelson, arXiv:0901.1145 [hep-ph]; U. Chattopadhyay, D. Das and D. P. Roy, arXiv:0902.4568 [hep-ph]; S. Bhattacharya and J. Chakraborty, arXiv:0903.4196 [hep-ph]; S. P. Martin, *Phys. Rev. D* **79**, 095019 (2009) doi:10.1103/PhysRevD.79.095019 [arXiv:0903.3568 [hep-ph]].
- [19] D. Matalliotakis and H. P. Nilles, *Nucl. Phys.* **B435**, 115(1995); M. Olechowski and S. Pokorski, *Phys. Lett.* **B344**, 201(1995); N. Polonski and A. Pomerol, *Phys. Rev.* **D51**, 6532(1995); P. Nath and R. Arnowitt, *Phys. Rev. D* **56**, 2820 (1997); E. Accomando, R. L. Arnowitt, B. Dutta and Y. Santoso, *Nucl. Phys. B* **585**, 124 (2000) doi:10.1016/S0550-3213(00)00321-7 [hep-ph/0001019]; J. R. Ellis, K. A. Olive and Y. Santoso, *Phys. Lett. B* **539**, 107 (2002) [arXiv:hep-ph/0204192]; H. Baer, A. Mustafayev, S. Profumo, A. Belyaev and X. Tata, *JHEP* **0507**, 065 (2005) [arXiv:hep-ph/0504001]; U. Chattopadhyay and D. Das, *Phys. Rev. D* **79**, 035007 (2009) doi:10.1103/PhysRevD.79.035007 [arXiv:0809.4065 [hep-ph]].
- [20] K. L. Chan, U. Chattopadhyay and P. Nath, *Phys. Rev. D* **58**, 096004 (1998) doi:10.1103/PhysRevD.58.096004 [hep-ph/9710473].

- [21] J. L. Feng, K. T. Matchev and T. Moroi, Phys. Rev. Lett. **84**, 2322 (2000) doi:10.1103/PhysRevLett.84.2322 [hep-ph/9908309].
- [22] U. Chattopadhyay, A. Corsetti and P. Nath, Phys. Rev. D **68**, 035005 (2003) doi:10.1103/PhysRevD.68.035005 [hep-ph/0303201].
- [23] H. Baer, C. Balazs, A. Belyaev, T. Krupovnickas and X. Tata, JHEP **0306**, 054 (2003) doi:10.1088/1126-6708/2003/06/054 [hep-ph/0304303].
- [24] D. Feldman, G. Kane, E. Kuflik and R. Lu, Phys. Lett. B **704**, 56 (2011) doi:10.1016/j.physletb.2011.08.063 [arXiv:1105.3765 [hep-ph]].
- [25] S. Akula, M. Liu, P. Nath and G. Peim, Phys. Lett. B **709**, 192 (2012) doi:10.1016/j.physletb.2012.01.077 [arXiv:1111.4589 [hep-ph]].
- [26] G. G. Ross, K. Schmidt-Hoberg and F. Staub, JHEP **1703**, 021 (2017) doi:10.1007/JHEP03(2017)021 [arXiv:1701.03480 [hep-ph]].
- [27] T. Ibrahim and P. Nath, Rev. Mod. Phys. **80**, 577 (2008) doi:10.1103/RevModPhys.80.577 [arXiv:0705.2008 [hep-ph]].
- [28] P. Nath and P. Fileviez Perez, Phys. Rept. **441**, 191 (2007) doi:10.1016/j.physrep.2007.02.010 [hep-ph/0601023].
- [29] M. Liu and P. Nath, Phys. Rev. D **87**, no. 9, 095012 (2013) doi:10.1103/PhysRevD.87.095012 [arXiv:1303.7472 [hep-ph]].
- [30] E. Arganda, J. L. Diaz-Cruz and A. Szykman, Eur. Phys. J. C **73**, no. 4, 2384 (2013) doi:10.1140/epjc/s10052-013-2384-z [arXiv:1211.0163 [hep-ph]].
- [31] E. Arganda, J. Lorenzo Diaz-Cruz and A. Szykman, Phys. Lett. B **722**, 100 (2013) doi:10.1016/j.physletb.2013.04.001 [arXiv:1301.0708 [hep-ph]].
- [32] B. Kaufman, P. Nath, B. D. Nelson and A. B. Spisak, Phys. Rev. D **92**, 095021 (2015) doi:10.1103/PhysRevD.92.095021 [arXiv:1509.02530 [hep-ph]].
- [33] P. Nath and A. B. Spisak, Phys. Rev. D **93**, no. 9, 095023 (2016) doi:10.1103/PhysRevD.93.095023 [arXiv:1603.04854 [hep-ph]].
- [34] A. Aboubrahim, P. Nath and A. B. Spisak, Phys. Rev. D **95**, no. 11, 115030 (2017) doi:10.1103/PhysRevD.95.115030 [arXiv:1704.04669 [hep-ph]].
- [35] J. R. Ellis, T. Falk and K. A. Olive, Phys. Lett. B **444**, 367 (1998) doi:10.1016/S0370-2693(98)01392-6 [hep-ph/9810360]; J. R. Ellis, T. Falk, K. A. Olive and M. Srednicki, Astropart. Phys. **13**, 181 (2000) Erratum: [Astropart. Phys. **15**, 413 (2001)] doi:10.1016/S0927-6505(99)00104-8 [hep-ph/9905481].
- [36] T. Nihei, L. Roszkowski and R. Ruiz de Austri, JHEP **0207**, 024 (2002) doi:10.1088/1126-6708/2002/07/024 [hep-ph/0206266].

- [37] H. Baer, T. Krupovnickas, A. Mustafayev, E. K. Park, S. Profumo and X. Tata, JHEP **0512**, 011 (2005) doi:10.1088/1126-6708/2005/12/011 [hep-ph/0511034]; H. Baer, T. Krupovnickas and X. Tata, JHEP **0406**, 061 (2004) doi:10.1088/1126-6708/2004/06/061 [hep-ph/0405058].
- [38] R. L. Arnowitt, B. Dutta, A. Gurrola, T. Kamon, A. Krislock and D. Toback, Phys. Rev. Lett. **100**, 231802 (2008) doi:10.1103/PhysRevLett.100.231802 [arXiv:0802.2968 [hep-ph]]; R. L. Arnowitt, A. Aurisano, B. Dutta, T. Kamon, N. Koley, P. Simeon, D. A. Toback and P. Wagner, Phys. Lett. B **649**, 73 (2007). doi:10.1016/j.physletb.2007.03.043
- [39] D. Feldman, Z. Liu and P. Nath, Phys. Rev. D **80**, 015007 (2009) doi:10.1103/PhysRevD.80.015007 [arXiv:0905.1148 [hep-ph]].
- [40] S. Akula and P. Nath, Phys. Rev. D **87**, no. 11, 115022 (2013) doi:10.1103/PhysRevD.87.115022 [arXiv:1304.5526 [hep-ph]].
- [41] J. E. Camargo-Molina, B. O’Leary, W. Porod and F. Staub, JHEP **1312**, 103 (2013) doi:10.1007/JHEP12(2013)103 [arXiv:1309.7212 [hep-ph]]; J. E. Camargo-Molina, B. Garbrecht, B. O’Leary, W. Porod and F. Staub, Phys. Lett. B **737**, 156 (2014) doi:10.1016/j.physletb.2014.08.036 [arXiv:1405.7376 [hep-ph]].
- [42] K. Kowalska, L. Roszkowski, E. M. Sessolo and A. J. Williams, JHEP **1506**, 020 (2015) doi:10.1007/JHEP06(2015)020 [arXiv:1503.08219 [hep-ph]].
- [43] A. Flrez, L. Bravo, A. Gurrola, C. vila, M. Segura, P. Sheldon and W. Johns, Phys. Rev. D **94**, no. 7, 073007 (2016) doi:10.1103/PhysRevD.94.073007 [arXiv:1606.08878 [hep-ph]].
- [44] J. Dutta, P. Konar, S. Mondal, B. Mukhopadhyaya and S. K. Rai, JHEP **1601**, 051 (2016) doi:10.1007/JHEP01(2016)051 [arXiv:1511.09284 [hep-ph]].
- [45] M. Berggren, A. Cakir, D. Krcker, J. List, I. A. Melzer-Pellmann, B. Safarzadeh Samani, C. Seitz and S. Wayand, Eur. Phys. J. C **76**, no. 4, 183 (2016) doi:10.1140/epjc/s10052-016-3914-2 [arXiv:1508.04383 [hep-ph]].
- [46] M. Berggren, PoS ICHEP **2016**, 154 (2016) [arXiv:1611.04450 [hep-ph]].
- [47] T. J. LeCompte and S. P. Martin, Phys. Rev. D **85**, 035023 (2012) doi:10.1103/PhysRevD.85.035023 [arXiv:1111.6897 [hep-ph]].
- [48] V. Khachatryan *et al.* [CMS Collaboration], Phys. Rev. Lett. **118**, no. 2, 021802 (2017) doi:10.1103/PhysRevLett.118.021802 [arXiv:1605.09305 [hep-ex]].
- [49] V. Khachatryan *et al.* [CMS Collaboration], Phys. Lett. B **767**, 403 (2017) doi:10.1016/j.physletb.2017.02.007 [arXiv:1605.08993 [hep-ex]].
- [50] L. Morvaj [ATLAS Collaboration], PoS EPS **-HEP2013**, 050 (2013).

- [51] A. Avetisyan *et al.*, arXiv:1308.1636 [hep-ex].
- [52] B. C. Allanach, Comput. Phys. Commun. **143**, 305 (2002) doi:10.1016/S0010-4655(01)00460-X [hep-ph/0104145].
- [53] B. C. Allanach, S. P. Martin, D. G. Robertson and R. Ruiz de Austri, Comput. Phys. Commun. **219**, 339 (2017) doi:10.1016/j.cpc.2017.05.006 [arXiv:1601.06657 [hep-ph]].
- [54] G. Blanger, F. Boudjema, A. Pukhov and A. Semenov, Comput. Phys. Commun. **192**, 322 (2015) doi:10.1016/j.cpc.2015.03.003 [arXiv:1407.6129 [hep-ph]].
- [55] A. Buckley, Eur. Phys. J. C **75**, no. 10, 467 (2015) doi:10.1140/epjc/s10052-015-3638-8 [arXiv:1305.4194 [hep-ph]].
- [56] L. E. Ibanez and G. G. Ross, Comptes Rendus Physique **8**, 1013 (2007) doi:10.1016/j.crhy.2007.02.004 [hep-ph/0702046 [HEP-PH]].
- [57] G. Belanger, S. Kraml and A. Pukhov, Phys. Rev. D **72**, 015003 (2005) doi:10.1103/PhysRevD.72.015003 [hep-ph/0502079].
- [58] F. E. Paige, S. D. Protopopescu, H. Baer and X. Tata, hep-ph/0312045.
- [59] G. Aad *et al.* [ATLAS Collaboration], Phys. Rev. D **93**, no. 5, 052002 (2016) doi:10.1103/PhysRevD.93.052002 [arXiv:1509.07152 [hep-ex]].
- [60] The ATLAS collaboration [ATLAS Collaboration], ATLAS-CONF-2016-096.
- [61] The ATLAS collaboration [ATLAS Collaboration], ATLAS-CONF-2017-039.
- [62] S. Dimopoulos, S. Raby and F. Wilczek, Phys. Rev. D **24**, 1681 (1981); J. Ellis, S. Kelley and D. V. Nanopoulos, Phys. Lett. **249B**, 441 (1990); **B260**, 131 (1991); U. Amaldi, W. de Boer and H. Furstenau, Phys. Lett. **260B**, 447 (1991); P. Langacker and M. x. Luo, Phys. Rev. D **44**, 817 (1991); L. J. Hall and U. Sarid, Phys. Rev. Lett. **70**, 2673 (1993); T. Dasgupta, P. Mamales and P. Nath, Phys. Rev. D **52**, 5366 (1995);
- [63] J. Alwall *et al.*, JHEP **1407**, 079 (2014) doi:10.1007/JHEP07(2014)079 [arXiv:1405.0301 [hep-ph]].
- [64] A. Djouadi, M. M. Muhlleitner and M. Spira, Acta Phys. Polon. B **38**, 635 (2007) [hep-ph/0609292].
- [65] T. Sjstrand *et al.*, Comput. Phys. Commun. **191**, 159 (2015) doi:10.1016/j.cpc.2015.01.024 [arXiv:1410.3012 [hep-ph]].
- [66] J. de Favereau *et al.* [DELPHES 3 Collaboration], JHEP **1402**, 057 (2014) doi:10.1007/JHEP02(2014)057 [arXiv:1307.6346 [hep-ex]].
- [67] I. Antcheva *et al.*, Comput. Phys. Commun. **182**, 1384 (2011). doi:10.1016/j.cpc.2011.02.008

- [68] The ATLAS collaboration [ATLAS Collaboration], ATLAS-CONF-2017-022.
- [69] The ATLAS collaboration [ATLAS Collaboration], ATLAS-CONF-2017-038.
- [70] CMS Collaboration [CMS Collaboration], CMS-PAS-SUS-14-021.
- [71] C. G. Lester and D. J. Summers, Phys. Lett. B **463**, 99 (1999) doi:10.1016/S0370-2693(99)00945-4 [hep-ph/9906349].
- [72] A. Barr, C. Lester and P. Stephens, J. Phys. G **29**, 2343 (2003) doi:10.1088/0954-3899/29/10/304 [hep-ph/0304226].
- [73] C. G. Lester and B. Nachman, JHEP **1503**, 100 (2015) doi:10.1007/JHEP03(2015)100 [arXiv:1411.4312 [hep-ph]].
- [74] R. M. Chatterjee, M. Guchait and D. Sengupta, Phys. Rev. D **86**, 075014 (2012) doi:10.1103/PhysRevD.86.075014 [arXiv:1206.5770 [hep-ph]].
- [75] H. Pagels and J. R. Primack, Phys. Rev. Lett. **48**, 223 (1982). doi:10.1103/PhysRevLett.48.223
- [76] H. Eberl and V. C. Spanos, JHEP **1308**, 055 (2013) doi:10.1007/JHEP08(2013)055 [arXiv:1305.6934 [hep-ph]].
- [77] H. Eberl and V. C. Spanos, Comput. Phys. Commun. **202**, 310 (2016) doi:10.1016/j.cpc.2015.12.027 [arXiv:1509.09159 [hep-ph]].
- [78] E. W. Kolb and M. S. Turner, Front. Phys. **69**, 1 (1990).
- [79] J. R. Ellis, J. E. Kim and D. V. Nanopoulos, Phys. Lett. **145B**, 181 (1984). doi:10.1016/0370-2693(84)90334-4
- [80] G. F. Giudice, A. Riotto and I. Tkachev, JHEP **9911**, 036 (1999) doi:10.1088/1126-6708/1999/11/036 [hep-ph/9911302].
- [81] M. Bolz, A. Brandenburg and W. Buchmuller, Nucl. Phys. B **606**, 518 (2001) Erratum: [Nucl. Phys. B **790**, 336 (2008)] doi:10.1016/S0550-3213(01)00132-8, 10.1016/j.nuclphysb.2007.09.020 [hep-ph/0012052].
- [82] K. Kohri, M. Yamaguchi and J. Yokoyama, Phys. Rev. D **72**, 083510 (2005) doi:10.1103/PhysRevD.72.083510 [hep-ph/0502211].
- [83] R. Allahverdi, S. Hannestad, A. Jokinen, A. Mazumdar and S. Pascoli, hep-ph/0504102.
- [84] V. S. Rychkov and A. Strumia, Phys. Rev. D **75**, 075011 (2007) doi:10.1103/PhysRevD.75.075011 [hep-ph/0701104].
- [85] J. Pradler and F. D. Steffen, Phys. Rev. D **75**, 023509 (2007) doi:10.1103/PhysRevD.75.023509 [hep-ph/0608344].

- [86] J. Pradler and F. D. Steffen, Phys. Lett. B **648**, 224 (2007) doi:10.1016/j.physletb.2007.02.072 [hep-ph/0612291].
- [87] R. Arya, N. Mahajan and R. Rangarajan, Phys. Lett. B **772**, 258 (2017) doi:10.1016/j.physletb.2017.06.038 [arXiv:1608.03386 [astro-ph.CO]].
- [88] M. Y. Khlopov and A. D. Linde, Phys. Lett. **138B**, 265 (1984). doi:10.1016/0370-2693(84)91656-3
- [89] M. Y. Khlopov, A. Barrau and J. Grain, Class. Quant. Grav. **23**, 1875 (2006) doi:10.1088/0264-9381/23/6/004 [astro-ph/0406621].
- [90] A. Addazi and M. Khlopov, Mod. Phys. Lett. A **31**, no. 19, 1650111 (2016) doi:10.1142/S021773231650111X [arXiv:1604.07622 [hep-ph]].
- [91] L. E. Strigari, New J. Phys. **11**, 105011 (2009) doi:10.1088/1367-2630/11/10/105011 [arXiv:0903.3630 [astro-ph.CO]].
- [92] M. Schumann, EPJ Web Conf. **96**, 01027 (2015) doi:10.1051/epjconf/20159601027 [arXiv:1501.01200 [astro-ph.CO]].
- [93] P. Cushman *et al.*, arXiv:1310.8327 [hep-ex].
- [94] P. Nath, Phys. Rev. Lett. **66**, 2565 (1991). doi:10.1103/PhysRevLett.66.2565; Y. Kizukuri and N. Oshimo, Phys. Rev. D **46**, 3025 (1992). doi:10.1103/PhysRevD.46.3025
- [95] T. Ibrahim and P. Nath, Phys. Lett. B **418**, 98 (1998) doi:10.1016/S0370-2693(97)01482-2, 10.1016/S0370-2693(99)00797-2 [hep-ph/9707409]; Phys. Rev. D **57**, 478 (1998) doi:10.1103/PhysRevD.58.019901, 10.1103/PhysRevD.60.079903, 10.1103/PhysRevD.60.119901, 10.1103/PhysRevD.57.478 [hep-ph/9708456]. Phys. Rev. D **58**, 111301 (1998) doi:10.1103/PhysRevD.60.099902, 10.1103/PhysRevD.58.111301 [hep-ph/9807501]; T. Falk and K. A. Olive, Phys. Lett. B **439**, 71 (1998) doi:10.1016/S0370-2693(98)01022-3 [hep-ph/9806236]; M. Brhlik, G. J. Good and G. L. Kane, Phys. Rev. D **59**, 115004 (1999) doi:10.1103/PhysRevD.59.115004 [hep-ph/9810457].
- [96] D. Feldman, Z. Liu, P. Nath and G. Peim, Phys. Rev. D **81**, 095017 (2010) doi:10.1103/PhysRevD.81.095017 [arXiv:1004.0649 [hep-ph]].
- [97] D. J. E. Marsh, Phys. Rept. **643**, 1 (2016) doi:10.1016/j.physrep.2016.06.005 [arXiv:1510.07633 [astro-ph.CO]]; J. E. Kim and D. J. E. Marsh, Phys. Rev. D **93**, no. 2, 025027 (2016) doi:10.1103/PhysRevD.93.025027 [arXiv:1510.01701 [hep-ph]]; L. Hui, J. P. Ostriker, S. Tremaine and E. Witten, Phys. Rev. D **95**, no. 4, 043541 (2017) doi:10.1103/PhysRevD.95.043541 [arXiv:1610.08297 [astro-ph.CO]]; J. Halverson, C. Long and P. Nath, arXiv:1703.07779 [hep-ph].